Early-Paleogene magmatism in the Pinaleño Mountains, Arizona: evidence for crustal melting of diverse basement assemblages during the Laramide Orogeny

Shane H. Scoggin[1*], James B. Chapman[1], Jessie E. Shields[1], Adam E. Trzinski[1], Mihai. N. Ducea[2, 3]

[1]Department of Geology and Geophysics, University of Wyoming, Laramie, WY 82071, USA

[2]Department of Geosciences, University of Arizona, Tucson, AZ, 85721, USA

[3]Faculty of Geology and Geophysics, University of Bucharest, 010041, Bucharest, Romania

*Corresponding author: Shane H. Scoggin (sscoggi2@uwyo.edu)

Telephone: 307-766-3386. Fax: 307-766-6679

Keywords: Anatexis; geothermometry; isotope geochemistry; zircon geochronology

ABSTRACT

Granitic rocks, interpreted to be related to crustal melting, were emplaced into regions of thickened crust in southern Arizona during the Laramide orogeny (80–40 Ma). Laramide-age anatectic rocks are exposed as plutons, sills, and dike networks that are commonly found in the exhumed footwalls of metamorphic core complexes. This study investigates newly discovered exposures of granodioritic–leucogranitic rocks from three intrusive phases in the footwall of the Pinaleño-Jackson Mountain metamorphic core complex of southeastern Arizona, called the Relleno suite. Zircon U-Pb geochronology indicates that the suite was emplaced from 58 to 52 Ma. Zircon Lu/Hf isotope geochemistry, whole rock Sr and Nd isotope geochemistry, and mineral O isotope geochemistry was used to investigate the source of these rocks and evaluate whether they are related to crustal anatexis. Average zircon $\varepsilon Hf_{(t)}$ values of the suite range from -4.7 to -7.9, whole rock $\varepsilon Nd_{(i)}$ and $^{87}Sr/^{86}Sr_{(i)}$ values range from -9.4 to -11.9 and 0.7064 to 0.7094, and quartz $\delta^{18}O_{VSMOW}$ values range from 6.8‰ to 9.4‰. Isotopic and geochemical data of these rocks are consistent with derivation from and assimilation of intermediate–mafic (meta)igneous rocks, at deep crustal levels and is supported by thermodynamic melt models of Proterozoic igneous rocks equivalent to those exposed in the Pinaleño Mountains. In comparison to other Laramide-age anatectic granites in southeast Arizona, those exposed in the Pinaleño Mountains are temporally similar but present compositional and isotopic differences which reflect melting and assimilation of different lithologies, producing distinct mineralogical and isotopic characteristics. The results suggest that crustal melting during this interval was not limited to metasedimentary protoliths and may have affected large portions of the deep crust. The early-Paleogene Relleno suite in the Pinaleño Mountains strengthens the relationship between crustal melting and regions of thickened crust associated with the Sevier and Laramide orogenies.

INTRODUCTION

The magmatic record in Cordilleran orogenic systems provides first-order insights into igneous processes including arc magmatism and anatexis. Southern Arizona, in the southern U.S. Cordillera, contains a rich magmatic history and most Phanerozoic collision-related igneous suites have been informally grouped based on their age and the tectonic environment they formed in. These groups include: 1) the Jurassic continental arc, 2) the Laramide arc; a Late-

Cretaceous to Early-Eocene continental arc, and 3) magmatism associated with the mid-Cenozoic ignimbrite flare-up (Haxel et al., 1984; Lang & Titley, 1998; Best et al., 2016; Chapman et al., 2018; Favorito & Seedorff, 2018). A lesser-known magmatic event in southern Arizona is the intrusion of peraluminous two-mica ± garnet granites during the early-Paleogene (Keith et al., 1980; Wright & Haxel, 1982; Haxel et al., 1984; Anderson et al., 1988; Goodwin & Haxel, 1990; Gehrels & Smith, 1991; Fornash et al., 2013; Ducea et al., 2020). These peraluminous rocks are mineralogically and geochemically distinct from other igneous rock types in southern Arizona and have been hypothesized to have formed by partial melting of Proterozoic metasedimentary and (meta)igneous basement rocks (Farmer & DePaolo, 1984; Haxel et al., 1984; Goodwin & Haxel, 1990; Fornash et al., 2013; Chapman et al., 2021). These rocks are interpreted to have originated by partial melting of the deeper crust of an orogenic plateau with thick crust (Chapman et al., 2020) during a period of low-angle to flat slab subduction of the Farallon plate when the locus of Laramide arc magmatism was migrating or had already migrated to the east (Coney & Reynolds, 1977; Constenius et al., 2003; Chapman et al., 2018; Seedorff et al., 2019).

In this study, we document and report on the occurrence of a Paleocene–Eocene metaluminous to weakly-peraluminous suite of rocks in the Pinaleño Mountains, which we refer to as the Relleno suite. Similar igneous suites are found in the Catalina-Rincon core complex (Wilderness suite), the Coyote Mountains core complex (Pan Tak granite), the Pozo Verde core complex (granite of Presumido Peak), and two-mica ± garnet granites exposed in the Sierra Blanca and Comobabi Mountains core complexes within the Tohono O'odham nation (Fig. 1) (Keith et al., 1980; Wright & Haxel, 1982; Haxel et al., 1984; Goodwin & Haxel, 1990; Force, 1997; Spencer et al., 2003, Ferguson et al., 2003). Collectively, we refer to these rocks as the southern Arizona anatectic suite. The timing of extension and exhumation of metamorphic core complexes in southern Arizona has been previously dated to Oligocene–Miocene time, post-dating this magmatic event by 15–25 Myr (Creasey et al., 1977; Foster et al., 1993; Long et al., 1995; Fayon et al., 2000; Terrien, 2012; Gottardi et al., 2020; Ducea et al., 2020; Jepson et al., 2021; Scoggin et al., 2021). Geochronological and geochemical studies of this suite of rocks have identified potential melt sources and protoliths including the Pinal Schist and Oracle granite, with lines of evidence including inherited Proterozoic zircon cores, evolved zircon $\varepsilon Hf_{(t)}$ values, evolved whole rock $\varepsilon Nd_{(i)}$ and $^{87}Sr/^{86}Sr_{(i)}$ values, elevated aluminum saturation indices

(ASI), and mineralogy consistent with melting and assimilation of pelitic and igneous protoliths (Wright & Haxel, 1982; Goodwin & Haxel, 1990; Fornash et al., 2013). We present new geochronological, geochemical, and isotopic data from intrusive rocks in the footwall of the Pinaleño-Jackson Mountain metamorphic core complex in order to evaluate the origin and source of the Relleno suite and evaluate whether it may also be a part of the southern Arizona anatectic suite.

GEOLOGIC SETTING

The Pinaleño Mountains

The Pinaleño Mountains compose part of the footwall of the Pinaleño-Jackson Mountain metamorphic core complex, which is the easternmost of a series of core complexes that trend NW–SE across southern Arizona (Crittenden et al., 1980; Davis & Hardy, 1981; Spencer, 1984) (Fig. 1). Slip on low-angle detachment faults associated with core complexes in southeastern Arizona is predominantly of Oligocene–Miocene age (e.g., Long et al., 1995; Fayon et al. 2000; Gottardi et al., 2019; Gottardi et al., 2020; Scoggin et al., 2021), is responsible for the exhumation of mid-crustal rocks (e.g., Anderson et al., 1988), and accommodated up to tens of kilometers of horizontal extension (Coney, 1980; Crittenden et al., 1980; Coney & Harms, 1984; Arca et al., 2010). The Pinaleño Mountains are bounded to the east by the NW–SE striking Pinaleño detachment fault which is buried in the Safford Basin and bounded to the west by the NW–SE Eagle Pass detachment fault that separates the syn-extensional ca. 27 Ma Galiuro Volcanics and associated volcanoclastic rocks from Paleo–Mesoproterozoic (meta)igneous basement rocks (Davis & Hardy 1981; Thorman & Naruk, 1987) (Fig. 2). Mylonitic rocks in the eastern range front of the Pinaleño Mountains have been correlated to mylonitic rocks from the Black Rock detachment fault on Jackson Mountain, located 10 km north of the Pinaleño Mountains, leading to interpretations of one continuous detachment fault along the eastern side of the Pinaleño and Santa Teresa Mountains (Crittenden et al., 1980; Davis, 1980; Davis & Hardy, 1981; Naruk, 1987; Long et al., 1995; Bailey & Eyster, 2003). Rocks exposed in the footwall of the Pinaleño Mountains core complex include 1) sparse outcrops of the mafic/volcanic member of ca. 1.7 Ga Pinal Schist, comprising greenschist and lower amphibolite metamorphic facies mineral assemblages (Cooper & Silver, 1964; Copeland & Condie, 1986; Eisele & Isachsen, 2001; Meijer, 2014); 2) variably metamorphosed (granodioritic–leucogranitic) ca. 1.6 Ga Pinaleño Mountains gneiss (equivalent to the Johnny Lyon

granodiorite; Silver, 1955; Thorman & Naruk, 1987); 3) ca. 1.4 Ga intrusions of the Oracle granite (Shride, 1967; Thorman, 1981); 4) ca. 1.1 Ga dolerite dikes (Bright et al., 2014); and 5) the ca. 55 Ma Relleno suite which intrudes Proterozoic igneous lithologies in the northeast range front (Long et al., 1995; this study) (Fig. 2, Fig. 3).

Basement rocks in Arizona constitute multiple accreted terranes which young eastward across Arizona from 2.2 to 1.6 Ga and produced crustal blocks with distinctive lithologic and isotopic characteristics. Crustal blocks of Arizona include the 2.2 Ga Mojave province, the 1.8–1.7 Ga Yavapai terrane, and the 1.7–1.6 Ga Mazatzal terrane (Farmer & DePaolo, 1983; Farmer & DePaolo, 1984; Karlstrom & Bowring, 1988; Chamberlain & Bowring, 1990; Dickinson & Lawton, 2001; Eisele & Isachsen, 2001). Southeastern Arizona, including the Pinaleño Mountains region, lies within the Cochise Block of the Mazatzal terrane (Copeland & Condie, 1986; Keep, 1996; Eisele & Isachsen, 2001). Mesoproterozoic igneous rocks including intrusions of A-type granite (e.g., Oracle granite; Anderson & Bender, 1989; Anderson & Morrison, 2005) and to a lesser extent, intrusions of dolerite (e.g., Bright et al., 2014) also forms a considerable volume of basement rock in southeastern Arizona.

Late-Cretaceous–Early-Cenozoic Magmatism in the Southern U.S. Cordillera

At the latitude of southern Arizona, continental arc magmatism migrated inland (eastward) during the Laramide orogeny (80–40 Ma), reaching modern-day New Mexico and Texas (Coney & Reynolds, 1977; Constenius et al., 2003; Chapman et al., 2018). Intrusions associated with the Laramide arc are calc-alkaline, metaluminous to peraluminous with molar A/CNK (aluminum saturation index, ASI) values of 0.7 to 1.2, are intermediate (50–70 wt. % SiO_2) in composition (Fig. 4), contain two feldspars and biotite ± amphibole with accessory minerals including titanite and allanite, usually have extrusive equivalents, and have radiogenic isotopic ratios reflecting a mantle source with assimilation of local basement rocks (Keith et al., 1980; Farmer & DePaolo, 1984; Lang & Titley, 1998; Fornash et al., 2013; Chapman et al., 2018; Seedorf et al., 2019). At any specific location, intrusions of the Laramide arc are generally older than the southern Arizona anatectic suite, however, the timing of these two distinct magmatic events overlap in the early-Eocene. There is temporal overlap between magmatism in the Pinaleño Mountains with nearby Laramide intrusions including the Morenci porphyry ca. 62–55 Ma and the Safford porphyry ca. 62–58 Ma (Lang & Titley, 1998).

Rocks of the southern Arizona anatectic suite are texturally and compositionally distinct from the Laramide continental arc. They have more evolved radiogenic isotopic compositions, are moderately to strongly-peraluminous with ASI values ≥ 1.1, are silica-rich (> 70 wt. % SiO_2), are plagioclase-rich with biotite ± muscovite ± garnet, lack extrusive equivalents, and were emplaced as plutons or sill/dike injection complexes (Keith et al., 1980; Miller & Bradfish, 1980; Haxel et al., 1984; Miller & Barton 1990; Fornash et al., 2013; Chapman et al., 2021; this study). The Wilderness suite in the Santa Catalina-Rincon Mountains and the Pan Tak Granite in the Coyote Mountains are two of the most well-known examples of peraluminous (two-mica ± garnet) granites in southern Arizona. The Wilderness suite was emplaced as sills (cumulative exposed thickness of 4–6 km) during multiple injection episodes from ca. 60 to 45 Ma (Keith et al., 1980; Fornash et al., 2013; Davis et al., 2019; Ducea et al, 2020). The Wilderness suite granites have ASI values ≥ 1.1, average zircon $\varepsilon Hf_{(t)}$ values < -10 and whole rock $\varepsilon Nd_{(i)}$ values < -10, and contain abundant ca. 1.4 Ga inherited cores in zircons, suggesting a significant contribution of ancient-crustal source rock: mainly Oracle granite but also potentially the Pinal Schist (Keith et al., 1980; Fornash et al., 2013). The ~58 Ma, peraluminous, two-mica ± garnet Pan Tak granite intrudes Proterozoic (meta)igneous, metasedimentary rocks, and Jurassic continental arc rocks in the footwall of the Coyote Mountains core complex (Wright & Haxel, 1982; Gottardi et al., 2020). The Pan Tak granite is also silica-rich (> 70 wt. % SiO_2) and comprises meters-thick dike networks that extend outward from a pluton in the center of the Coyote Mountains. Previous studies hypothesized that the Pan Tak granite was derived from the Pinal Schist and/or the Jurassic arc of southern Arizona (Wright & Haxel, 1982; Haxel et al., 1984).

PETROGRAPHY

Geologic mapping was undertaken to define the extent of the Relleno suite. It outcrops as a small pluton (approximately 10 km^2) cut by two generations of dikes in Ash Creek Canyon and extends northwest to Shingle Mill Canyon on the eastern side of the Pinaleño Mountains (Fig. 2). The easternmost parts of the intrusion are mylonitized. The intrusion was previously mapped by Thorman & Naruk (1987) as the middle-Proterozoic Granodiorite of White Streaks Canyon. We explored other regions of the eastern Pinaleño Mountains but did not find equivalent rocks, although there may be other exposures. The intrusions can be divided into three phases. Phase 1 is the main plutonic body that is roughly circular in shape and includes several smaller satellite

plutons. Phase 2 is a set of leucogranite dikes that cross-cut Phase 1 rocks. Phase 3 is another set of leucogranite dikes that cross-cuts both Phase 1 and Phase 2 rocks (Fig. 3). Five igneous rock samples of the Relleno suite and six igneous rocks samples of Proterozoic basement lithologies were collected for isotopic, geochronological, geochemical, and petrographic analysis.

The Relleno Suite

Intrusions from the Relleno suite comprise plagioclase in greater abundance than K-feldspar, quartz and biotite with apatite, magnetite, and zircon, with two samples containing muscovite in small quantities (Fig. 5). Minor sericitic alteration of feldspars and epidote/chlorite alteration of biotite is locally present. Intrusions from the Relleno suite can resemble lithologies of the Pinaleño Mountains gneiss and Oracle granite (*i.e.*, leucocratic–pegmatitic, biotite gneisses, and granites lacking amphibole), and can be difficult to distinguish in locations with high densities of dikes and country rock of similar composition.

Sample ASH-1A was collected from the Phase 1 plutonic body of the Relleno suite. Phase 1 is more mafic than other phases of the Relleno suite (66 wt. % SiO_2); it is a weakly-foliated biotite granodiorite that contains amphibolite enclaves and is increasingly gneissic and mylonitized to the east. Sample ASH-1A comprises plagioclase (30 %), quartz (25 %), biotite (20%), K-feldspar (15%), with magnetite/opaque oxide, apatite and zircon (5%), and minor epidote and chlorite (< 5%). Phase 2 of the Relleno suite is represented by granitic samples ASH-1B, ASH-2, and SS-20-06. Samples ASH-1B and ASH-2 comprise granitic and pegmatitic dikes up to 1.5 m in width that cross-cut the Phase 1 pluton and surrounding Proterozoic country rock. Samples ASH-1B and ASH-2 contain plagioclase (40%), quartz (35%), K-feldspar (10%), biotite (5%), apatite, zircon and opaque oxide (< 5%), and epidote/chlorite alteration of biotite (< 5%). A few grains of muscovite intergrown with biotite are present in sample ASH-2. Sample SS-20-06 was collected from a densely-concentrated network of dikes up to 2 meters wide west of the Phase 1 pluton which cross-cuts dolerite and Johnny Lyon granodiorite (Fig. 3). Dolerite appears as partially melted enclaves within the outcrop from which sample SS-20-06 was collected. Sample SS-20-06 is similar in composition (72 wt. % SiO_2) and mineralogy to other Phase 2 samples and comprises plagioclase (40%), quartz (30%), K-feldspar (10%), biotite (10%), apatite and zircon (5%), epidote and chlorite (< 5%), and opaque oxide (< 1%), but contains more apatite, as well as sparse muscovite. Sample ASH-1L was collected from Phase 3

of the Relleno suite which is manifest as aplitic leucogranite dikes (74.5 wt. % SiO_2) up to one meter wide that cross-cuts the Phase 1 pluton and dikes of Phase 2. Sample ASH-1L is similar in composition to Phase 2 and comprises quartz (50%), plagioclase (35%), K-feldspar (10%), and trace biotite, opaque oxide, and apatite/zircon (< 5%) but has finer-grained quartz and plagioclase crystals compared to Phase 1 and 2.

Zircons from samples representing each phase of the Relleno suite were selected for textural and compositional analysis with back scatter electron (BSE) and cathodoluminescence imagery (CL). Zircons from Phase 1 of the Relleno suite (sample ASH-1A) are relatively large (200–500 μm length), euhedral zircons that display subtle shading differences indicating rim/core compositional variability, but are not strongly zoned, and contain abundant and/or large inclusions that appear dark in CL. Phase 2 zircons (samples ASH-1B, ASH-2, and SS-20-06) are on average smaller (lengths < 300 μm) than Phase 1 zircons. They display stronger oscillatory zoning patterns, and contain inclusions of apatite. Zircons from Phase 3 of the Relleno suite comprise heterogeneous size populations (75–600 μm length), and a mixture of strongly-oscillatory zoned and un-zoned zircons.

Proterozoic Basement Rocks

Six samples were selected for geochemical and U-Pb analyses from distinct Paleo–Mesoproterozoic intrusions. Samples SS-20-03 and SS-20-12 are equivalent to the Johnny Lyon granodiorite; sample SS-20-03 comprises plagioclase, quartz and biotite with K-feldspar and opaque oxide and sample SS-20-12 comprises porphyritic K-feldspar with coarse-grained biotite, plagioclase, quartz, muscovite, and minor titanite, apatite, and zircon. Samples SS-20-08, SS-20-09, and SS-20-10 come from intrusions of Oracle granite. Sample SS-20-08 comprises coarse-grained quartz and plagioclase with minor biotite, K-feldspar and magnetite. Samples SS-20-09 and SS-20-10 are foliated and come from pegmatitic dikes which cross-cut gneissic Johnny Lyon granodiorite. Samples SS-20-09 and SS-20-10 are strongly-peraluminous granites and comprise coarse-grained quartz and plagioclase with large muscovite grains and minor biotite. Sample SS-20-04 comes from a dolerite enclave that comprises olivine, plagioclase, clinopyroxene, and opaque oxide with apatite, and abundant secondary epidote, biotite, and chlorite. Sample ASH-A was collected in Ash Creek Canyon and is a gneissic amphibole-biotite-plagioclase enclave representative of the amphibolite enclaves present in Phase 1 of the Relleno suite.

METHODS

Zircons from rock samples were separated using standard methods including crushing and grinding, a Wilfley table, magnetic, and heavy liquid separation. Zircons and relevant geochronology standards were mounted in epoxy and polished to expose the interior of the crystals. Epoxy mounts were imaged with a Gatan Chroma CL2 CL detector and BSE imagery on a Hitachi 3400N scanning electron microscope (SEM) at the University of Arizona LaserChron facility. Locations for U-Pb, trace element, and Lu-Hf analyses from zircon crystals were chosen using a combination of CL and BSE images. The same zircons were analyzed for U-Pb geochronology, trace element and Lu-Hf isotope geochemistry (Supplementary Data File 1, Supplementary Data File 2). In situ isotopic analyses of U, Pb and Hf along with trace element and rare earth element analyses were collected by LA-ICP-MS at the University of Arizona LaserChron Center using a Teledyne Photon Machines G2^{TM} solid state NeF excimer laser paired with either a Nu Instruments multicollector mass spectrometer or Thermo Fisher E2^{TM} single-collector mass spectrometer. Zircon U-Pb analytical standards used include R33 (age range = 399–439 Ma), FC (age range = 1004–1199 Ma), and SL(age range = 532–587 Ma). The value, uncertainty, and range of zircon Lu-Hf analytical standards used include FC ($^{176}Hf/^{177}Hf$ = 0.28218 ± 0.00005, 0.28208–0.28269), R33 ($^{176}Hf/^{177}Hf$ = 0.28275 ± 0.00003, 0.28266–0.28288), Plešovice ($^{176}Hf/^{177}Hf$ = 0.28250 ± 0.00004, 0.28245–0.28277), Temora ($^{176}Hf/^{177}Hf$ = 0.28267 ± 0.00003, 0.28259–0.28274), Mud Tank ($^{176}Hf/^{177}Hf$ = 0.28254 ± 0.00003, 0.28247–0.28259), and 91500 ($^{176}Hf/^{177}Hf$ = 0.28232 ± 0.00005, 0.28219–0.28275). Lu-Hf analyses were conducted using a 40 µm beam diameter, a repetition rate of 7 Hz, and laser fluence of approximately 2 J/cm^2. Trace element analyses included simultaneous measurement of 23 trace and rare earth elements along with U-Th-Pb isotopes to determine spot age. Measured trace element isotopes include ^{27}Al, ^{29}Si, ^{31}P, ^{45}Sc, ^{49}Ti, ^{89}Y, ^{93}Nb, ^{139}La, ^{140}Ce, ^{141}Pr, ^{146}Nd, ^{152}Sm, ^{153}Eu, ^{157}Gd, ^{159}Tb, ^{164}Dy, ^{165}Ho, ^{166}Er, ^{169}Tm, ^{174}Yb, ^{175}Lu, ^{177}Hf, ^{181}Ta, ^{202}Hg, ^{204}(Hg+Pb), $^{206,207,208}Pb$, ^{232}Th, and ^{235}U. Dwell times of these elements range from 0.001–0.3 s. Trace element analyses were conducted with 30 µm beam diameter, a repetition rate of 7 Hz, and laser fluence of ~7 J/cm^2, which yields pits approximately 20 µm deep. Analytical standards for zircon trace elements were normalized to ^{29}Si and include natural zircon standards 91500, MAD-559, and synthetic standard NIST 612. Data reduction of zircon U-Pb, Lu-Hf, and trace element analyses

follows the procedures outlined by Gehrels et al. (2008), Cecil et al. (2011), Gehrels & Pecha (2014), and Chapman et al. (2016) using AGEcalc, HfcalcML, and TREEcalc.

Rock samples were pulverized with a tungsten carbide puck mill grinder and homogenized with alkali flux fusion. Major elements were analyzed via X-ray fluorescence spectroscopy and trace elements were analyzed via ICP-MS by ALS Geochemistry. Whole rock powders were used to analyze isotopes of Sr and Nd via ID-TIMS at the University of Arizona following the procedures outlined in Otamendi et al. (2009) and Girardi et al. (2012). Powders were put in Savillex vials and dissolved in hot concentrated HF-HNO_3. After dissolution, unmixed Caltech Rb, Sr, and mixed Sm-Nd spikes were added to the samples (Ducea & Saleeby, 1998). Rb, Sr, and REEs were separated in AG50W-X4 resin ion exchange columns using 1–4 M HCl. Separation of Sm and Nd was achieved in anion exchange columns containing LN Spec resin using 0.1–2.5 N HCl. Rb was loaded onto Re filaments using silica gel and H_3PO_4. Sr was loaded onto Ta filaments with Ta_2O_5 powder. Sm and Nd were loaded onto Re filaments using platinized carbon and resin beads. Mass spectrometric analyses were completed on a VG Sector 54 multicollector instrument fitted with adjustable 10^{11} Faraday collectors and a Daly photomultiplier (Otamendi et al., 2009). Isotope dilution calculations were carried out using an off-line manipulation program. Analyses consisted of acquisitions of 100 isotopic ratios. The average result of five analyses of standard NRbAAA performed during this study is $^{85}Rb/^{87}Rb$ = 2.61311 ± 0.00018. Five analyses of NIST standard NBS987 yield mean $^{87}Sr/^{86}Sr$ ratio of 0.710259 ± 0.000004 and $^{84}Sr/^{86}Sr$ = 0.056434 ± 0.000011. Five analyses of Sm standard Sm929 yield $^{148}Sm/^{147}Sm$ = 0.74880 ± 0.00023 and $^{148}Sm/^{152}Sm$ = 0.42111 ± 0.00007. Five analyses of Nd standard LaJolla yield the following ratios: $^{142}Nd/^{144}Nd$ = 1.14184 ± 0.00002, $^{143}Nd/^{144}Nd$ = 0.511853 ± 0.000002, $^{145}Nd/^{144}Nd$ = 0.348390 ± 0.000002, and $^{150}Nd/^{144}Nd$ = 0.23638 ± 0.00002. The Sr isotope ratios of standards and samples were normalized to $^{86}Sr/^{88}Sr$ = 0.1194 and Nd isotope ratios were normalized to $^{146}Nd/^{144}Nd$ 0.7219. Estimated analytical uncertainties (± 2σ) are $^{87}Rb/^{86}Sr$ = 0.35%, $^{87}Sr/^{86}Sr$ = 0.0014%, $^{147}Sm/^{144}Nd$ = 0.4% and $^{143}Nd/^{144}Nd$ = 0.0012%. Procedural blanks averaged from five analyses were 10 pg Rb, 150 pg Sr, 2.7 pg Sm and 5.5 pg Nd.

Oxygen isotope ratios were determined via laser fluorination at the University of Texas High Temperature Stable Isotope Lab following the procedures outlined by Sharp (1990). Rock

samples were crushed and sieved and mineral separates were picked under binocular microscope and washed in dilute HCl and deionized water. Approximately 2 milligrams of sample was heated with a CO_2 laser in the presence of BrF_5 and cryogenically purified in a silicate extraction line. Oxygen isotopes were measured on a dual-inlet Thermo Scientific MAT253 stable isotope ratio mass spectrometer (IRMS) using the UWG-2 garnet standard ($\delta^{18}O_{VMSOW}$ = 5.8 ± 0.1‰, n = 5) from Valley et al. (1995), and in-house quartz standard Lausanne 1. All $\delta^{18}O$ values are reported relative to VSMOW with reproducibility better than ± 0.1‰.

Pseudosection models of Proterozoic country rock were constructed using Perple_X version 6.9 (Connolly, 1990; 2005; 2009). Equilibrium mineral assemblages and melt chemistry were evaluated at end-member conditions of 725 °C, 5 kbar and 825 °C, 10 kbar to illustrate the possible differences in melt chemistry and melt volume. The range of model temperatures is based on thermometry data (see below). The range of model pressures is not constrained by this study, but based on pressure estimates from the Wilderness suite (Anderson et al., 1988). For starting compositions, we used whole rock geochemistry data from Johnny Lyon granodiorite samples SS-20-03 and SS-20-12, Oracle granite samples SS-20-09, SS-20-10, and KB90-111 (from Barovich, 1991), and dolerite samples SS-20-04 and 09PL5 (from Bright et al., 2014). Models were generated using the 10-component NCKFMASHTO (Na_2O-CaO-K_2O-FeO-MgO-Al_2O_3-SiO_2-H_2O-TiO_2-O_2) compositional system, the thermodynamic dataset of Holland & Powell (2011), and the following solution models; feldspar (Fuhrman & Lindsley, 1988), Bi(W), Mica(W), and melt(W) (White et al., 2014). Specifically, we attempted to model the most mafic end-member (Phase 1, ~66 wt. % SiO_2) in the Relleno suite under the assumption that Phases 2 and 3 can be produced from Phase 1 by fractional crystallization. Water content for melt models of Johnny Lyon granodiorite and Oracle granite are based on modal mineralogy (i.e., hydrous mineral content) and was < 1 wt. % H_2O.

RESULTS

Isotopic and Elemental Analyses of Zircon

Ages from zircon U-Pb analyses are reported as weighted mean ages of concordant analyses for crystallization ages and upper and or lower discordia intercept ages for discordant samples. Uncertainty for crystallization ages are reported at 2σ, calculated by adding in quadrature instrumental uncertainty determined during the analysis run and standard deviation of zircon

ages from a single sample. All samples of the Relleno suite yield concordant ages except sample ASH-1A that exhibits reverse discordance (Fig. 6). Zircons from Phase 1 (sample ASH-1A) yield an average age of 54.9 ± 1.5 Ma (n = 17). Zircons from Phase 2 include samples SS-20-06, ASH-1B, and ASH-2 which yield weighted mean ages of 56.1 ± 2.1 Ma (MSWD = 5.5; n = 23), 55.3 ± 2.1 Ma (MSWD = 5.5; n = 21), and 55.4 ± 2.0 Ma (MSWD = 5.8; n = 21) respectively. Zircons from Phase 3 (sample ASH-1L) yield a weighted mean age of 54.5 ± 2.2 Ma (MSWD = 4.7; n = 21) (Table 1, Fig. 6). These new ages are in agreement with two single-grain zircon U-Pb analyses from a biotite granite (sample PM-3) referenced in Long et al. (1995) of 56.9 ± 0.3 Ma (1σ) and 57.1 ± 0.3 Ma (1σ). Zircon U-Pb ages of all phases of the Relleno suite overlap within uncertainty, although cross-cutting relationships indicate relative timing (Fig. 3).

Zircons from sample SS-20-12 yield a crystallization age of 1638 ± 6 Ma (MSWD = 1.0; n = 20) and zircons from sample SS-20-03 yield a discordia upper intercept age of 1621 ± 5 Ma and a lower intercept age of 70 ± 38 Ma (MSWD = 4.7; n = 23). Zircons from samples SS-20-08, SS-20-09, and SS-20-10 yield discordia upper intercept ages of 1445 ± 5 Ma (MSWD = 2.1; n = 19), 1443 ± 4 Ma (MSWD = 0.9; n = 37), and 1455 ± 6 Ma (MSWD = 3.3; n = 39) respectively. Zircons from samples SS-20-09 and SS-20-10 yield discordia lower intercept ages of 30 ± 81 Ma and 1150 ± 38 Ma. Lower discordia intercept ages of samples SS-20-03 and SS-20-09 overlap within uncertainty for the crystallization age of the Relleno suite and the discordance in these samples is interpreted to be related to Pb-loss during that intrusion event. Zircons from sample SS-20-04 yield a discordia upper intercept age of 1612 ± 16 Ma and a lower intercept age of 1116 ± 19 Ma (MSWD = 7.1; n = 17). The lower intercept age for this sample is interpreted to be the crystallization age, consistent with ages reported by Bright et al. (2014), and the upper intercept is interpreted to reflect analyses of inherited zircon cores, presumably from the Johnny Lyon granodiorite (Table 1, Fig. 7).

Trace element analyses of zircon were performed on samples SS-20-06 (n = 9), ASH-1A (n = 9), ASH-1L (n = 9), and ASH-2 (n = 7) and are only reported for zircons with U-Pb ages consistent with the crystallization age of the sample. Rare earth element concentrations of zircon from the Relleno suite show large positive Ce anomalies in all samples and small to no negative Eu anomalies. All samples display a concave slope with depletions in LREEs and enrichments HREEs, however, sample SS-20-06 is enriched in MREE and HREES compared to other

samples. U/Th values of zircons are in the range 1.0–1.8 (ASH-1A), 1.9–4.4 (SS-20-06), 1.3–8.6 (ASH-2), and 1.2–3.6 (ASH-1L) and increase with decreasing Ti-in-zircon crystallization temperature (Table 3, Fig, 8, Supplementary Data File 1). We used the Ti-in-zircon thermometer of Ferry & Watson (2007) to estimate temperatures of zircon crystallization. We used $a\mathrm{SiO_2} = 1$ and $a\mathrm{TiO_2} = 0.6$ in melt following the recommendation of Schiller & Finger (2019) due to the absence of Ti phases like titanite, rutile, and/or ilmenite in the Relleno suite. Ti concentrations in zircons range from 0.9 to 9.6 ppm and are summarized in Table 3. Resulting Ti-in-zircon crystallization temperatures range from 673 °C to 752 °C. Loucks et al. (2020) present a Ti-in-zircon thermometer with pressure dependence, and using emplacement depths of ~15 km calculated from the Wilderness suite by Anderson et al. (1988), the temperature estimations of the Relleno suite are higher than the calibration presented by Ferry & Watson (2007) and range from 720 °C to 802 °C, however, better constraints on emplacement depth of anatectic granites from southern Arizona are needed. Zircon saturation temperatures following Watson & Harrison (1983) were calculated for rock samples from each phase of the Relleno suite and range from 714 °C to 792 °C. Zircon saturation temperatures were also calculated for Wilderness suite samples WILD-1 and WILD-2 which yield temperatures of 727 °C and 710 °C respectively. Ti-in-zircon crystallization temperatures of the Relleno suite are similar to zircon saturation temperatures for samples ASH-1A and ASH-1L, but samples SS-20-06 and ASH-2 display zircon saturation temperatures 50–125 °C higher than Ti-in-zircon crystallization temperatures.

We used Ce, U, and Ti concentrations of zircon to estimate the oxidation state of the Relleno suite following the zircon oxybarometer of Loucks et al. (2020) which is applicable over a range of magmatic types and conditions, including metaluminous–peraluminous granitic magmas. Redox state of a magma can change Ce^{3+} to Ce^{4+} in oxidizing conditions which increases Ce compatibility in zircon. Ce concentrations in zircon range from 4.1 to 47.6 ppm and U concentrations range from 38 to 2,106 ppm. Using pressure estimates of emplacement of the Wilderness suite from Anderson et al. (1988) zircons from the Relleno suite yield a range of ΔFMQ values from 0.2 to 2.6 and average ΔFMQ values of 1.5 to 2.1, equivalent to a range of log $f\mathrm{O_2}$ values from -16 to -14 (Table 3).

Zircon $\varepsilon\mathrm{Hf_{(t)}}$ values are reported as weighted averages with uncertainty reported at 2σ. Zircon $\varepsilon\mathrm{Hf_{(t)}}$ values were calculated from grains consistent with the crystallization age of the

sample (Table 1, Fig. 9). Sample ASH-1A yields the most juvenile $\varepsilon Hf_{(t)}$ value of -4.7 ± 2.4 (n = 12), samples ASH-1L and ASH-2 yield similar $\varepsilon Hf_{(t)}$ values of -5.8 ± 4.9 (n = 11) and -5.8 ± 2.7 (n = 10). Sample SS-20-06 yields the most evolved $\varepsilon Hf_{(t)}$ value of -7.9 ± 5.3 (n = 11).

Whole Rock Major and Trace Element Geochemistry

The Relleno suite samples are metaluminous to moderately peraluminous and have ASI values (molar $Al_2O_3/CaO-3.33*P_2O_5+Na_2O+K_2O$) of 0.99–1.05 and represent M values (molar $Na_2O+K_2O+2*CaO/Al_2O_3*SiO_2$) of 1.39–1.67, have alkali contents of 7–8 wt. % and a range of silica content of 66–75 wt. %. (Fig. 4). For comparison we collected and analyzed two samples of the Wilderness suite granites (WILD-1 and WILD-2), they have similar alkali and silica content but have higher ASI values of 1.1 and 1.3 and represent M values of 1.15 and 1.25. The Relleno suite samples display a convex chondrite-normalized REE pattern with enrichments in LREEs, moderate depletions in HREEs, a flat HREE slope, and weak to no negative Eu anomaly. Wilderness suite samples have similar LREE concentrations, more pronounced negative Eu anomalies and a slight enrichment in HREEs relative to the Relleno suite. On a MORB-normalized trace element diagram the Relleno and Wilderness suites show negative anomalies for Nb, P, and Ti (Fig. 4).

Whole Rock Sr and Nd Isotopes

We measured whole rock Sr and Nd isotopes from Relleno suite samples ASH-1A, ASH-1B, ASH-2, SS-20-06, ASH-1L, and amphibolite enclave sample ASH-A (Table 1). Initial isotope ratios are reported from their U-Pb crystallization ages or recalculated to 55 Ma. The Relleno suite displays a range of $^{87}Sr/^{86}Sr_{(0)}$ values of 0.706687–0.709639 resulting in $^{87}Sr/^{86}Sr_{(i)}$ values of 0.706448–0.709352 and $^{143}Nd/^{144}Nd_{(0)}$ values of 0.512243–0.512124 resulting in $^{143}Nd/^{144}Nd_{(i)}$ values of 0.512207–0.512087 and $\varepsilon Nd_{(i)}$ values from -9.4 to -11.8 (Table 1, Fig. 9, Fig. 10). Amphibolite enclave sample ASH-A yields an $^{87}Sr/^{86}Sr_{(55\ Ma)}$ value of 0.7084 and an $\varepsilon Nd_{(55\ Ma)}$ value of -3.0.

Mineral Oxygen Isotopic Compositions

Oxygen isotopic data are presented from quartz, feldspar, biotite, magnetite, and zircon in Table 4. Reconstructed whole rock $\delta^{18}O_{VSMOW}$ values range from 6.4–7.1‰. Sample SS-20-06 yields a quartz $\delta^{18}O_{VSMOW}$ value ~ 2‰ heavier relative to other samples of 9.4‰ and sample ASH-1L yields a biotite $\delta^{18}O$ value 3–4‰ lower than other samples. Using quartz-magnetite, quartz-

zircon, and quartz-biotite mineral pairs, oxygen isotope equilibration thermometry was applied to samples following Bottinga & Javoy (1975) and Javoy (1977). Quartz-biotite, quartz-magnetite, and quartz-zircon equilibration temperatures of the Relleno suite are in the range 483–781 °C, 525–708 °C, and 664 °C respectively (Fig. 11).

Pseudosection Models

Modeled melt compositions are presented for representative samples of Oracle granite, dolerite, and Johnny Lyon granodiorite (Fig. 11, Supplementary File 3). At conditions of 725 °C and 5 kbar dolerite did not produce any melt, however, samples of Johnny Lyon granodiorite and Oracle granite produce melt compositions of 69–71 wt. % SiO_2, 6–9 wt. % Na_2O+K_2O, ASI values of 1.0–1.17, and one granodiorite sample produced an Fe/Mg value of 5.6. Melt percentages of Johnny Lyon granodiorite are 7–9 wt. % and melt percentages of Oracle granite are 5–12 wt. %. At conditions of 825 °C and 10 kbar, dolerite produced melt compositions in the range 62–70 wt. % SiO_2, 3–6 wt. % Na_2O+K_2O, ASI values of 1.02 and Fe/Mg values of 3–7 while Johnny Lyon granodiorite and Oracle granite produce melt compositions with ranges of 67–71 wt. % SiO_2, 6.5–9 wt. % Na_2O+K_2O, ASI values of 1.0–1.07, Fe/Mg values of 3–9. Melt percentages are 3.5–22 wt. % for dolerite, 8–9 wt. % for Johnny Lyon granodiorite, and 5–12 wt. % for Oracle granite. Melting of dolerite requires up to 5 wt. % added H_2O at 825 °C.

DISCUSSION

New zircon U-Pb geochronology reveals that the Relleno suite is contemporaneous with both the southern Arizona anatectic suite and the Laramide continental arc, however, the geochemical and isotopic compositions of the Relleno suite do not match well with either magmatic event. Laramide arc rocks are generally interpreted to have originated in the mantle and the experienced various degrees of crustal assimilation and fractional crystallization in MASH (melting, assimilation, storage, homogenization) (Hildreth & Moorbath, 1988) or deep crustal hot zones (Annen et al., 2006). Rocks from the southern Arizona anatectic suite are thought to be chiefly produced during crustal anatexis with no new mass additions from the mantle. We favor the interpretation that the Relleno suite is primarily a crustal melt that was derived from a mixture of intermediate–mafic lithologies in the lower to middle crust, specifically, equivalents of the 1.6 Ga Johnny Lyon granodiorite and 1.1 Ga dolerite which the Relleno suite intruded into. Melting of these igneous rocks can explain the unique geochemical characteristics and also distinguishes

the Relleno suite from other parts of the southern Arizona anatectic suite that have been interpreted to be derived in part from metasedimentary sources. The disparity between the geochemical and isotopic characteristics between the Wilderness and Relleno suites results from the regional distribution of metasedimentary and igneous basement-rock lithologies in southern Arizona. In the following sections, we discuss the characteristics and features that lead us to this conclusion.

Evidence for Crustal Melting

Radiogenic Isotopes

Whole rock Nd isotopes of the Relleno suite are strongly indicative of melting and assimilation of evolved crustal material. $\varepsilon Nd_{(i)}$ values range from -9.4 to -11.8 and are slightly more evolved than $\varepsilon Nd_{(i)}$ values of the Wilderness suite, which range from -8.4 to -10.2. The Relleno and Wilderness suites are more evolved than Laramide arc intrusions such as the Leatherwood granodiorite in the Catalina-Rincon core complex, which has $\varepsilon Nd_{(i)}$ values of -4 to -8 (Fornash et al., 2013) and most other Laramide arc intrusions in southern Arizona, which range in $\varepsilon Nd_{(i)}$ from +1 to -10 (Farmer & DePaolo, 1984; Lang & Titley, 1998) (Fig. 10). Intrusions of the Laramide arc display isotopic signatures consistent with mixing of mantle and crustal sources. In contrast, intrusions of the southern Arizona anatectic suite, including the Wilderness and Relleno suites, show significantly more evolved $\varepsilon Nd_{(i)}$ values, indicative of negligible mantle influence. Despite the evolved $\varepsilon Nd_{(i)}$ values, the Relleno suite displays only moderately evolved $^{87}Sr/^{86}Sr_{(i)}$ values of 0.7064–0.7094, which we interpret to reflect partial derivation from a relatively mafic crustal source depleted in Rb and radiogenic Sr. We performed a mixing calculation using Sr and Nd concentrations and isotopic compositions between potential source rocks for the Relleno suite (Fig. 10) and the suite plots on a mixing line between 1.1 Ga dolerite and Johnny Lyon granodiorite. The calculations suggest the Relleno suite could have been produced by partial melting of a mixed source comprising 80–55 % dolerite and 45–20 % granodiorite, however, sericitic alteration of feldspar and chlorite/epidote alteration of biotite produced by fluids associated with Oligocene–Miocene detachment faulting and core complex exhumation may have altered the Sr (and/or O) isotopic compositions of the Relleno suite, producing Sr isotopic values that artificially resemble a greater magnitude of assimilation of lithologies depleted in radiogenic Sr (e.g., 1.1 Ga dolerite).

Zircon Lu-Hf isotopes from the Relleno suite yield $\varepsilon Hf_{(t)}$ values of -4.7 to -7.9 and are also consistent with a crustal source, however, $\varepsilon Hf_{(t)}$ values are juvenile compared to the Wilderness suite (Fig. 9a). $\varepsilon Hf_{(t)}$ and $\varepsilon Nd_{(i)}$ values of the Relleno suite display a positive deviation from the terrestrial array of Vervoort et al. (1999, 2000) (Fig. 9b). This type of positive deviation from the terrestrial array is often observed in igneous rocks produced by crustal anatexis (e.g., Zhang et al., 2019; Wang et al., 2020). Decoupling between the Hf and Nd isotopic systems during crustal melting has been attributed to disequilibrium melting and incomplete dissolution of mineral phases (Iles et al., 2018). Incomplete dissolution of low Lu/Hf zircon may result in melts with elevated $^{176}Hf/^{177}Hf$ relative to the bulk source rock composition (Watson & Harrison, 1983; Patchett et al., 1984; Scherer et al., 2000). This is particularly true for anatectic rocks produced from metasedimentary sources (Tang et al., 2014; Zhang et al., 2019). However, inherited (xenocrystic) zircon is relatively rare in the Relleno suite, which suggests that the parental magmas may have been at or below zircon saturation during initial melting (see section below on zircon inheritance). Another possibility is that oxide mineralogy exerts a control on Hf isotopic compositions during crustal melting. Schmitz et al. (2004) identified residual mafic lower crustal rocks (granulite facies xenoliths) in South Africa that were enriched in Lu/Hf during high-pressure metamorphism and crustal melting. The enrichment was attributed to the stability of titanomagnetite and ilmenite (which have Hf partition coefficients > 1), at the expense of rutile (Green & Pearson, 1986). Melts derived from similar deep crustal mafic rocks could produce the Hf-Nd decoupling observed in the Relleno suite. A final possibility is that preferential melting of a high Lu/Hf phase in the source could generate elevated $\varepsilon Hf_{(t)}$ values (Schmitz et al., 2004; Iles et al., 2018). Besides a high Lu/Hf oxide like ilmenite (e.g., Schmitz et al., 2004), other likely candidates include garnet, monazite, and apatite. The Relleno suite shows evidence for moderate HREE depletion (Fig. 4), which is interpreted to represent residual garnet or amphibole in the source, rather than preferential melting of garnet.

Oxygen Isotopes

Oxygen isotopes of the Relleno suite yield quartz $\delta^{18}O_{VSMOW}$ values of 6.8– 9.4‰ while intrusions of the Laramide arc in southern Arizona and northern Mexico range in quartz $\delta^{18}O_{VSMOW}$ of 9.5–11.8‰ (Turi & Taylor, 1971; Salas et al., 2013). Proterozoic rocks in southern Arizona including the Pinal Schist, Johnny Lyon granodiorite, and Oracle granite have quartz

$\delta^{18}O_{VSMOW}$ values of 11.7–15.1‰, 10.2–11.0‰ and 9.3–10.7‰ respectively (Turi & Taylor, 1971; Kerrich & Rehrig, 1987; Anderson et al., 2005). The Relleno suite displays quartz O isotope ratios considerably depleted in ^{18}O compared to Laramide arc and Proterozoic granitic rocks, which we interpret to reflect (partial) derivation from a mafic source, like the 1.1 Ga dolerite (Fig. 10).

Geothermometry

Zircon saturation temperatures, Ti-in-zircon temperatures, and O isotope equilibration temperatures from the Relleno suite are consistent with dehydration melting of muscovite- and biotite-bearing protoliths at mid-crustal depths (Stevens & Clemens, 1993; Vielzeuf & Montel, 1994; Patiño-Douce & Harris, 1998) (Fig. 11). Zircon-based thermometers (T_{zr} and Ti-in-zircon) tend to yield systematic underestimates of melt temperatures due to the late-crystallizing nature of zircon in granitic melts (Siegel et al., 2018; Barnes et al., 2019). Zr-based thermometers yield temperatures of 690–792 °C, which are interpreted to be minimum estimates of the melt temperature in the source region. Oxygen isotope thermometry from the Relleno suite (657–781 °C) is consistent with the range of Zr-based thermometers. Subsolidus quartz-biotite and quartz-magnetite equilibration temperatures from sample SS-20-06 (566 °C and 527 °C respectively) likely reflect post-crystallization alteration or isotopic disequilibrium between mineral phases, while the quartz-biotite temperature of 483 °C from sample ASH-1L reflects partial alteration/recrystallization of biotite to chlorite.

Age Relationships and Zircon Inheritance

Five new LA-ICP-MS zircon U-Pb ages from granitic rocks in the footwall of the Pinaleño Mountains indicate crystallization of the Relleno suite from 52.4 to 57.6 Ma (inclusive of age uncertainties). The relatively large uncertainty in the crystallization age reflects the large range of single zircon ages (ca. 60–50 Ma) measured in each sample. The large spread of zircon U-Pb ages observed within a single sample is similar to the Wilderness suite (Fornash et al., 2013; Davis et al., 2019) and is interpreted to represent a prolonged period of melt generation and possible reworking of intrusive rocks (Fig. 12), which is characteristic of anatectic magmatism (Howard et al., 2011; Weinberg, 2016; Chapman et al., 2021).

Inherited zircons from the Relleno suite are rare (n = 8/150), but the ages of inherited cores range from 1.68–1.25 Ga, consistent with assimilation of ca. 1.6 Ga Johnny Lyon

granodiorite and 1.1 Ga dolerite (which contained zircons of ca. 1.2 Ga age) and possibly 1.4 Ga Oracle granite, however, we note that xenocrystic zircon cores are the only line of evidence for assimilation of Oracle granite (Fig. 7). Similarly aged inherited zircon (1.7–1.4 Ga) are preserved in the Wilderness suite, which has been interpreted to be primarily derived from Oracle granite and Pinal Schist (Fornash et al., 2013). Bea et al. (2021) suggest that source rock lithology of anatectic melts control the magma volume and solubility of zircon, and that zircon dissolution kinetics might be a governing factor in zircon preservation and inheritance characteristics. Anatectic granites derived from a pelitic source display significantly higher percentages (~90% xenocrystic cores) of inherited zircon compared to rocks derived from a metaluminous igneous source (~10% xenocrystic cores) (Bea et al., 2021). It is also likely that the Relleno suite and other anatectic rocks derived from intermediate–mafic sources represent higher magmatic temperatures compared to those derived from pelitic sources, which was more likely to completely dissolve xenocrystic zircon (e.g., Miller et al., 2003).

Magmatic Sources

Proterozoic and Mesozoic igneous–metasedimentary lithologies compose a majority of the crustal section across southern Arizona and exert the strongest control on the isotopic, mineralogical, and geochemical characteristics of anatectic granites. Intrusions like the Pan Tak granite and Wilderness suite are hypothesized to have partially melted and assimilated pelitic lithologies of the Pinal Schist and exhibit strongly evolved $^{87}Sr/^{86}Sr_{(i)}$, $\varepsilon Nd_{(i)}$ and $\varepsilon Hf_{(t)}$ values, comprise two micas ± garnet and display elevated ASI values (Keith et al., 1980; Wright & Haxel, 1982; Force, 1997; Fornash et al., 2013). In contrast to these intrusions, the Relleno suite, is metaluminous to weakly-peraluminous, comprises granodioritic lithologies, and is interpreted to have partially melted and assimilated mafic crustal rocks based on highly evolved $\varepsilon Nd_{(i)}$ and $\varepsilon Hf_{(t)}$ values, but moderately evolved $^{87}Sr/^{86}Sr_{(i)}$ values and low quartz $\delta^{18}O$ values. We hypothesize that the mafic contribution to this suite comes from partial melting and assimilation of equivalents of the 1.1 Ga dolerite exposed in the Pinaleño Mountains and southeastern Arizona.

To test our hypothesis that partial melting of intermediate–mafic (meta)igneous lithologies could have contributed the Relleno suite we used pseudosection modeling to estimate melt compositions produced by partial melting of Johnny Lyon granodiorite, Oracle granite, and

dolerite (the majority of lithologies exposed in the Pinaleño Mountains). Specifically, we attempted to reproduce the Phase 1 composition, represented by sample ASH-1A – the most mafic sample in the Relleno suite, under the assumption that Phases 2 and 3 could be produced by fractional crystallization of Phase 1. Partial melting of Oracle granite does not produce compositions similar to the Relleno suite at either parameter we modeled (Fig. 11), which is consistent with the radiogenic isotope data and paucity of inherited zircon crystals with ca. 1.4 Ga U-Pb ages. The modeled compositions resulting from partial melting of Oracle granite are too enriched in alkalis and enriched in Fe/Mg to be a source of the Relleno suite (Fig. 11, Supplementary File 3).

The composition of Phase 1 of the Relleno suite can be reproduced by partial melting of a mixed source, consisting of dolerite and Johnny Lyon granodiorite, but only under specific P-T conditions and initial water contents. The results of the pseudosection modeling indicate that partial melting of the Johnny Lyon granodiorite can occur at both end-member P-T conditions considered and at water contents < 1 wt. %, however, partial melting of dolerite only occurs at the hotter and deeper end-member condition considered (825 °C and 10 kbar) and only occurs when the amount of water in the starting composition is increased to ~5% (Supplementary File 3). Because a free water phase is needed to partially melt dolerite at the pressure and temperature conditions considered, it raises the question as to where that water may have come from. There are many possible sources, but some possibilities include mineral dehydration during metamorphism, fluid exsolution during crystallization of other close by intrusions, and externally introduced water related to the dehydration of the shallowly subducting Farallon slab. Simple mixing models between representative dolerite sample (sample 09PL5) and a representative Johnny Lyon granodiorite sample (sample SS-20-03) suggests Phase 1 of the Relleno suite could represent a mixture comprising 60–70 % Johnny Lyon granodiorite and 30–40 % dolerite, based on SiO_2, alkali content, ASI, and Fe/Mg values (Fig. 11). These mixing models suggest a larger contribution of Johnny Lyon granodiorite than dolerite in the melt source of the Relleno suite compared to Sr/Nd isotopic mixing models, which suggest significantly more dolerite (55–80%) in the source.

An alternative interpretation to crustal melting is that the Relleno suite represents an intrusion of the Laramide continental arc which has been interpreted to have involved melts

generated in the continental mantle lithosphere (CML) and variable degrees of crustal assimilation in the southern U.S. Cordillera (Chapman et al., 2017; 2018). To examine this possibility the isotopic compositions of the CML were estimated from mantle lithosphere xenoliths in the Geronimo Volcanic Field, located ~70 km southwest of the Pinaleño Mountains (Kempton et al., 1991). The most juvenile isotopic compositions are interpreted to reflect end-member values for the CML. Sr/Nd mixing calculations between the CML and Proterozoic rocks produce $\varepsilon Nd_{(i)}$ values that are too juvenile for accompanying $^{87}Sr/^{86}Sr_{(i)}$ values to resemble the Relleno suite (Fig. 10). When coupled with other lines of evidence, including Sr/Nd isotopic compositions consistent with a mixture of dolerite and granodiorite in the source and zircon $\varepsilon Hf_{(t)}$ values that plot along 1.6–1.4 Ga crustal evolution lines, a mantle source for this suite can be discounted. However, Sr and O isotopic compositions strongly indicate the participation of mafic protolith(s) in the melt source, a hypothesis supported by whole rock Nd and Sr isotope data, zircon Lu-Hf isotope data, quartz $\delta^{18}O$ data, and melt composition calculations based on pseudosection modeling.

If our interpretation of the Relleno suite is correct, it suggests that other intermediate composition (e.g., 65–70 wt. % SiO_2) igneous suites in southern Arizona may also have been produced by crustal anatexis. For example the 58 Ma Texas Canyon stock, a quartz monzonite, located approximately 70 km southeast of the Pinaleño Mountains, is temporally and compositionally similar to the Relleno suite and was intruded into Johnny Lyon granodiorite and Pinal Schist (Turi & Taylor, 1971). The Texas Canyon stock is peraluminous, cross-cut by abundant aplite dikes, has strongly evolved radiogenic isotopes, heavy $\delta^{18}O_{VSMOW}$ values (Turi & Taylor, 1971; Chapman et al., 2018) and was previously interpreted by Arnold (1986) to be related to crustal melting, similar to the Wilderness suite. Parts of the Texas Canyon stock are strongly peraluminous and contain biotite + muscovite, however, the muscovite may be coarse muscovite or greisen alteration product and not magmatic (Runyon et al., 2019). Regardless, the Texas Canyon stock is an example of an intrusive unit that could also have been generated by partial melting of mafic (meta)igneous rocks in addition to other lithologies.

Petrogenetic and Tectonic Implications

Throughout the North American Cordillera, peraluminous two-mica ± garnet granites were emplaced into the middle crust during the Laramide Orogeny, but the petrogenetic and tectonic

processes that generated these crustal melts remain controversial (Miller & Bradfish, 1980; Miller & Barton, 1990; Chapman et al., 2021). Decompression melting during the exhumation of metamorphic core complexes has been proposed in the northern U.S. and southern Canadian Cordillera (e.g., Shuswap core complex: Vanderhaege et al., 1999; Teyssier & Whitney, 2002; Vanderhaege et al., 2003; Gordon et al., 2008). However, anatectic granitoids in southeastern Arizona pre-date the exhumation of metamorphic core complexes by 15–25 Ma, and are probably not directly related to the formation of metamorphic core complexes (Chapman et al., 2021). Lack of migmatites in the core complexes of southern Arizona compared to core complexes in the central and northern Cordillera suggests that anatexis may have taken place at deeper crustal levels than what is exposed in core complexes of southeastern Arizona. Barometric estimates completed by Anderson et al. (1988) suggest mid-crustal emplacement depths for the Wilderness suite in the Catalina and Rincon Mountains (~4 ± 1 kbar), and we suspect a similar range for the Relleno suite due to its temporal and spatial relationship to the Wilderness suite. Future studies on anatectic rock in southern Arizona and core complex exhumation depths will help resolve emplacement pressures for the southern Arizona anatectic suite. A more appealing model proposed to be related to the petrogenesis of anatectic rocks exposed in core complexes in the central U.S. Cordillera is crustal thickening and radiogenic heating (e.g., Patiño-Douce et al., 1990; McGrew et al., 2000; Lee et al., 2003). If southern Arizona was an orogenic plateau as suggested by Chapman et al. (2020), we hypothesize that elevated geothermal gradients and radiogenic heating of crustal rocks may be responsible for generating partial melts.

CONCLUSIONS

This study presents the first in-depth investigation of early-Paleogene granitic rocks in the Pinaleño-Jackson Mountain metamorphic core complex. New zircon U-Pb geochronology indicates that the Relleno suite was emplaced from 60 to 50 Ma. The range of ages from each sample/phase of the suite suggests a prolonged crystallization history, similar to the range of ages observed in the Wilderness suite in the Catalina Mountains (ca. 60–45 Ma). A wide range of magmatic ages (> 10 Myr) and inherited zircon cores are common features of igneous suites throughout the North American Cordilleran Anatectic Belt, and is consistent with a long-lived anatectic reservoir in the crustal root of an orogenic plateau (Whitney et al., 2013; Chapman et al., 2021). A compilation of ages from the Wilderness suite, Pan-Tak granite, and Relleno suite

suggests that the onset of crustal melting in the southern Arizona anatectic suite occurred at ~60 Ma. Whole rock $\varepsilon Nd_{(i)}$ and $^{87}Sr/^{86}Sr_{(i)}$ values and isotopic mixing models are consistent with a mixed source including the 1.6 Ga Johnny Lyon granodiorite and 1.1 Ga dolerite. Zircon $\varepsilon Hf_{(t)}$ values from the Relleno suite are also consistent with a crustal source, however, O isotopes of this suite strongly suggests input of a mafic source which we interpret to be 1.1 Ga dolerite. Hf-Nd isotopic decoupling (i.e., deviation from the Hf-Nd terrestrial array) also supports partial melting of crustal rocks and is in agreement with dolerite and granodiorite in the melt source of the Relleno suite. Zircon-based geothermometers and O isotope equilibration temperatures indicate magmatic temperatures consistent with dehydration melting of muscovite and biotite-bearing protoliths (~650–800 °C), however some mineral pairs yield temperatures below the modeled solidi for the Relleno suite. In conjunction with thermometric and isotopic data, thermodynamic melt models of Johnny Lyon granodiorite, Oracle granite, and dolerite suggest that melt compositions representing a mix between granodiorite and dolerite are similar to Phase 1 of the Relleno suite.

We suggest that the Relleno suite represents an intrusion of the southern Arizona anatectic suite which was emplaced into the Arizonaplano, an orogenic plateau with thick crust present in the southern U.S. Cordillera during the Laramide orogeny (Chapman et al., 2020). Intrusions such as the Wilderness suite and Pan Tak granite lie within the Pinal Basin, and their compositions and apparent magmatic volumes reflect derivation from and assimilation of metapelitic (+ igneous) rocks. The Pinaleño Mountains are located outside of the Pinal Basin, and the lower apparent magmatic volumes, isotopic compositions, and geochemical characteristics of the Relleno suite more strongly resemble partial melting and derivation from mafic igneous rocks. From these relationships we infer that the southern Arizona anatectic suite represents a regionally significant magmatic event, produced by melting of diverse basement lithologies in the crust. The southern Arizona anatectic suite is distinct from other Mesozoic–Cenozoic igneous rocks in the southern U.S. Cordillera, it generally post-dates and has distinct isotopic and mineralogical characteristics from intrusions of the Laramide continental arc, and is unrelated to the formation and exhumation of metamorphic core complexes.

ACKNOLWEGEMENTS

Scoggin acknowledges support from the University of Wyoming Department of Geology and Geophysics, the University of Wyoming College of Arts and Sciences, and the Geological Society of America. Chapman acknowledges support from U.S. National Science Foundation grant EAR-1928312. M.N.D. acknowledges support from the Romanian Executive Agency for Higher Education, Research, Development, and Innovation Funding project PN-III-P4-ID-PCCF-2016-0014. We thank Dr. Mark Pecha, Dr. Jaime Barnes, Dr. Martin Pepper, Dr. Sarah George, and Derek Hoffman for analytical assistance. We thank Dr. Arend Meijer for discussions and data that improved this manuscript. We thank Dr. Marlina Elburg for editorial handling, and Dr. Peter Schaaf and two anonymous reviewers whose comments greatly improved the manuscript.

DATA AVAILABILITY STATEMENT

All data presented in this article are available in the article and online supplementary material.

REFERENCES

Anderson, J.L., Barth, A.P. & Young, E.D. (1988). Mid-crustal Cretaceous roots of Cordilleran metamorphic core complexes. *Geology* 16, 366-369.

Anderson, J.L. & Bender, E.E. (1989). Nature and origin of Proterozoic A-type granitic magmatism in the southwestern United States of America. *Lithos* 23, 19-52.

Anderson, J.L. & Morrison, J. (2005). Ilmenite, magnetite, and peraluminous Mesoproterozoic anorogenic granites of Laurentia and Baltica. *Lithos* 80, 45-60.

Annen, C., Blundy, J.D. & Sparks, R.S.J. (2006). The genesis of intermediate and silicic magmas in deep crustal hot zones. *Journal of Petrology* 47, 505-539.

Arca, M.S., Kapp, P. & Johnson, R.A. (2010). Cenozoic crustal extension in southeastern Arizona and implications for models of core-complex development. *Tectonophysics* 488, 174-190.

Arnold, A.H. (1986). Geologic Implications of a Geo-Chemical Study of Three Two-Mica Granites in Southern Arizona. *Tucson, University of Arizona* (Masters Thesis).

Bailey, C.M. & Eyster, E.L. (2003). General shear deformation in the Pinaleño Mountains metamorphic core complex, Arizona. *Journal of Structural Geology* 25, 1883-1892.

Barnes, C.G., Werts, K., Memeti, V. & Ardill, K. (2019). Most granitoid rocks are cumulates: deductions from hornblende compositions and zircon saturation. *Journal of Petrology* 60, 2227-2240.

Barovich, K.M. (1991). Behavior of lutetium-hafnium, samarium-neodymium and rubidium-strontium isotopic systems during processes affecting continental crust. *Tucson, University of Arizona* (Doctoral dissertation, Ph. D. thesis).

Bea, F., Morales, I., Molina, J.F., Montero, P. & Cambeses, A. (2021). Zircon stability grids in crustal partial melts: implications for zircon inheritance. *Contributions to Mineralogy and Petrology* 176, 1-13.

Best, M.G., Christiansen, E.H., de Silva, S. & Lipman, P.W. (2016). Slab-rollback ignimbrite flareups in the southern Great Basin and other Cenozoic American arcs: A distinct style of arc volcanism. *Geosphere* 12, 1097-1135.

Bottinga, Y. & Javoy, M. (1975). Oxygen isotope partitioning among the minerals in igneous and metamorphic rocks. *Reviews of Geophysics* 13, 401-418.

Bright, R.M., Amato, J.M., Denyszyn, S.W. & Ernst, R.E. (2014). U-Pb geochronology of 1.1 Ga diabase in the southwestern United States: Testing models for the origin of a post-Grenville large igneous province. *Lithosphere* 6, 135-156.

Cecil, M.R., Gehrels, G., Ducea, M.N. & Patchett, P.J. (2011). U-Pb-Hf characterization of the central Coast Mountains batholith: Implications for petrogenesis and crustal architecture. *Lithosphere* 3, 247-260.

Chamberlain, K.R. and Bowring, S.A. (1990). Proterozoic geochronologic and isotopic boundary in NW Arizona. *The Journal of Geology* 98, 399-416.

Chapman, J.B., Gehrels, G.E., Ducea, M.N., Giesler, N. & Pullen, A. (2016). A new method for estimating parent rock trace element concentrations from zircon. *Chemical Geology* 439, 59-70.

Chapman, J.B., Ducea, M.N., Kapp, P., Gehrels, G.E. & DeCelles, P.G. (2017). Spatial and temporal radiogenic isotopic trends of magmatism in Cordilleran orogens. *Gondwana Research* 48, 189-204.

Chapman, J.B., Dafov, M.N., Gehrels, G., Ducea, M.N., Valley, J.W. & Ishida, A. (2018). Lithospheric architecture and tectonic evolution of the southwestern US Cordillera: Constraints from zircon Hf and O isotopic data. *Bulletin* 130, 2031-2046.

Chapman, J.B., Greig, R. & Haxel, G.B. (2020). Geochemical evidence for an orogenic plateau in the southern US and northern Mexican Cordillera during the Laramide orogeny. *Geology* 48, 164-168.

Chapman, J.B., Runyon, S.E., Shields, J., Lawler, B.L., Pridmore, C.J., Scoggin, S.H., Swaim, N.T., Trzinski, A.E., Wiley, H.N., Barth, A.P. & Haxel, G.B. (2021). The North American Cordilleran Anatectic Belt. *Earth-Science Reviews* 215.

Crittenden, M.D., Coney, P.J., Davis, G.H. and Davis, G.H. (1980). *Cordilleran metamorphic core complexes* (Vol. 153). Geological Society of America.

Coney, P.J. (1980). Cordilleran metamorphic core complexes: An overview. *Cordilleran metamorphic core complexes: Geological Society of America Memoir* 153, 7-31.

Coney, P.J. & Reynolds, S.J. (1977). Cordilleran benioff zones. *Nature* 270, 403-406.

Coney, P.J. & Harms, T.A. (1984). Cordilleran metamorphic core complexes: Cenozoic extensional relics of Mesozoic compression. *Geology* 12, 550-554.

Connolly, J.A.D. (1990). Multivariable phase diagrams; an algorithm based on generalized thermodynamics. *American Journal of Science* 290, 666-718.

Connolly, J.A. (2005). Computation of phase equilibria by linear programming: a tool for geodynamic modeling and its application to subduction zone decarbonation. *Earth and Planetary Science Letters* 236, 524-541.

Connolly, J.A.D. (2009). The geodynamic equation of state: what and how. *Geochemistry, Geophysics, Geosystems* 10.

Constenius, K.N., Esser, R.P. & Layer, P.W. (2003). Extensional collapse of the Charleston-Nebo salient and its relationship to space-time variations in Cordilleran orogenic belt tectonism and continental stratigraphy. Rocky Mountain Section (SEPM).

Cooper, J.R. & Silver, L.T. (1964). *Geology and ore deposits of the Dragoon quadrangle, Cochise County, Arizona* (No. 416).

Copeland, P. & Condie, K.C. (1986). Geochemistry and tectonic setting of lower Proterozoic supracrustal rocks of the Pinal Schist, southeastern Arizona. *Geological Society of America Bulletin* 97, 1512-1520.

Creasey, S.C., Banks, N.G., Ashley, R.P. & Theodore, T.G. (1977). Middle Tertiary plutonism in the Santa Catalina and Tortolita Mountains, Arizona. *US Geol. Surv., J. Res* 5, 705-717.

Davis, G.H. & Hardy JR, J.J. (1981). The Eagle Pass detachment, southeastern Arizona: Product of mid-Miocene listric (?) normal faulting in the southern Basin and Range. *Geological Society of America Bulletin* 92, 749-762.

Davis, G.H., Spencer, J.E. & Gehrels, G.E. (2019). Field-trip guide to the Catalina-Rincon metamorphic core complex, Tucson, Arizona. *Geologic Excursions in Southwestern North America*, *55*.

Dickinson, W.R. & Lawton, T.F. (2001). Carboniferous to Cretaceous assembly and fragmentation of Mexico. *Geological Society of America Bulletin* 113, 1142-1160.

Drewes, H. (1996). Geology of Coronado National Forest. *US Geological Survey Bulletin* 2083, 17-41.

Ducea, M. & Saleeby, J. (1998). A case for delamination of the deep batholithic crust beneath the Sierra Nevada, California. *International Geology Review*, *40*(1), 78-93.

Ducea, M.N., Triantafyllou, A. & Krcmaric, J. (2020). New timing and depth constraints for the Catalina Metamorphic Core complex, Southeast Arizona. *Tectonics* 39.

Eisele, J. & Isachsen, C.E. (2001). Crustal growth in southern Arizona: U-Pb geochronologic and Sm-Nd isotopic evidence for addition of the Paleoproterozoic Cochise block to the Mazatzal province. *American Journal of Science* 301, 773-797.

Farmer, G.L. & DePaolo, D.J. (1983). Origin of Mesozoic and Tertiary granite in the western United States and implications for Pre-Mesozoic crustal structure: 1. Nd and Sr isotopic studies in the geocline of the Northern Great Basin. *Journal of Geophysical Research: Solid Earth* 88, 3379-3401.

Farmer, G.L. & Depaolo, D.J. (1984). Origin of Mesozoic and Tertiary granite in the western United States and implications for Pre-Mesozoic crustal structure: 2. Nd and Sr isotopic studies of unmineralized and Cu-and Mo-mineralized granite in the Precambrian Craton. *Journal of Geophysical Research: Solid Earth* 89, 10141-10160.

Favorito, D.A. & Seedorff, E. (2018). Discovery of Major Basement-Cored Uplifts in the Northern Galiuro Mountains, Southeastern Arizona: Implications for Regional Laramide Deformation Style and Structural Evolution. *Tectonics* 37, 3916-3940.

Fayon, A.K., Peacock, S.M., Stump, E. & Reynolds, S.J. (2000). Fission track analysis of the footwall of the Catalina detachment fault, Arizona: Tectonic denudation, magmatism, and erosion. *Journal of Geophysical Research: Solid Earth* 105, 11047-11062.

Ferguson, C.A., Demsey, K.A., Gilbert, W.G., House, P.K., Johnson, B.J., Maher, D.J., Richard, S.M., Skotnicki, S.J., Spencer, J.E. & Youberg, A. (2003). *Geologic Map of the Tortolita Mountains, Pinal and Pima Counties, Arizona*. Arizona Geological Survey.

Ferry, J.M. & Watson, E.B. (2007). New thermodynamic models and revised calibrations for the Ti-in-zircon and Zr-in-rutile thermometers. *Contributions to Mineralogy and Petrology* 154, 429-437.

Force E.R. (1997) Geology and mineral resources of the Santa Catalina Mountains, Southeastern Arizona: a cross-sectional approach. Monogr Miner Resour Sci No. 1. Center for Mineral Resources, University of Arizona, 135.

Fornash, K.F., Patchett, P.J., Gehrels, G.E. & Spencer, J.E. (2013). Evolution of granitoids in the Catalina metamorphic core complex, southeastern Arizona: U–Pb, Nd, and Hf isotopic constraints. *Contributions to Mineralogy and Petrology* 165, 1295-1310.

Foster, D.A., Gleadow, A.J., Reynolds, S.J. & Fitzgerald, P.G. (1993). Denudation of metamorphic core complexes and the reconstruction of the transition zone, west central Arizona: Constraints from apatite fission track thermochronology. *Journal of Geophysical Research: Solid Earth* 98, 2167-2185.

Fuhrman, M.L. & Lindsley, D.H. (1988). Ternary-feldspar modeling and thermometry. *American mineralogist* 73, 201-215.

Gehrels, G. & Pecha, M. (2014). Detrital zircon U-Pb geochronology and Hf isotope geochemistry of Paleozoic and Triassic passive margin strata of western North America. *Geosphere* 10, 49-65.

Gehrels, G.E., Valencia, V.A. & Ruiz, J. (2008). Enhanced precision, accuracy, efficiency, and spatial resolution of U-Pb ages by laser ablation–multicollector–inductively coupled plasma–mass spectrometry. *Geochemistry, Geophysics, Geosystems* 9.

Gehrels, G.E. & Smith, C.H. (1991). U-Pb geochronologic constraints on the age of thrusting, crustal extension, and peraluminous plutonism in the Little Rincon Mountains, southern Arizona. *Geology* 19, 238-241.

Girardi, J.D., Patchett, P.J., Ducea, M.N., Gehrels, G.E., Cecil, M.R., Rusmore, M.E., Woodsworth, G.J., Pearson, D.M., Manthei, C. & Wetmore, P. (2012). Elemental and isotopic evidence for granitoid genesis from deep-seated sources in the Coast Mountains Batholith, British Columbia. *Journal of Petrology* 53, 1505-1536.

Goodwin, L.B. & Haxel, G.B. (1990). Structural evolution of the Southern Baboquivari Mountains, south-central Arizona and north-central Sonora. *Tectonics* 9, 1077-1095.

Gordon, S.M., Whitney, D.L., Teyssier, C., Grove, M. & Dunlap, W.J. (2008). Timescales of migmatization, melt crystallization, and cooling in a Cordilleran gneiss dome: Valhalla complex, southeastern British Columbia. *Tectonics* 27.

Gottardi, R., Schaper, M.C., Barnes, J.D. & Heizler, M.T. (2018). Fluid–rock interaction and strain localization in the Picacho Mountains detachment shear zone, Arizona, USA. *Tectonics* 37, 3244-3260.

Gottardi, R., McAleer, R., Casale, G., Borel, M., Iriondo, A. & Jepson, G., 2020. Exhumation of the Coyote Mountains metamorphic core complex (Arizona): implications for orogenic collapse of the southern North American Cordillera. *Tectonics* 39.

Green, T.H. & Pearson, N.J. (1986). Rare-earth element partitioning between sphene and coexisting silicate liquid at high pressure and temperature. *Chemical Geology* 55, 105-119.

Haxel, G.B., Tosdal, R.M., May, D.J. & Wright, J.E. (1984). Latest Cretaceous and early Tertiary orogenesis in south-central Arizona: Thrust faulting, regional metamorphism, and granitic plutonism. *Geological Society of America Bulletin* 95, 631-653.

Hildreth, W. & Moorbath, S. (1988). Crustal contributions to arc magmatism in the Andes of central Chile. *Contributions to mineralogy and petrology* 98, 455-489.

Howard, K.A., Wooden, J.L., Barnes, C.G., Premo, W.R., Snoke, A.W. & Lee, S.Y. (2011). Episodic growth of a Late Cretaceous and Paleogene intrusive complex of pegmatitic leucogranite, Ruby Mountains core complex, Nevada, USA. *Geosphere* 75, 1220-1248.

Iles, K.A., Hergt, J.M. & Woodhead, J.D. (2018). Modelling isotopic responses to disequilibrium melting in granitic systems. *Journal of Petrology* 59, 87-113.

Javoy, M. (1977). Stable isotopes and geothermometry. *Journal of the Geological Society* 133, 609-636.

Jepson, G., Carrapa, B., George, S.W., Triantafyllou, A., Egan, S.M., Constenius, K.N., Gehrels, G.E. & Ducea, M.N., 2021. Resolving mid-to upper-crustal exhumation through apatite petrochronology and thermochronology. *Chemical Geology* 565.

Karlstrom, K.E. & Bowring, S.A. (1988). Early Proterozoic assembly of tectonostratigraphic terranes in southwestern North America. *The Journal of Geology* 96, 561-576.

Keep, M. (1996). The Pinal Schist, southeast Arizona, USA: contraction of a Palaeoproterozoic rift basin. *Journal of the Geological Society* 153, 979-993.

Keith, S.B., Reynolds, S., Damon, P.E., Shafiqullah, M., Livingston, D.E. & Pushkar, P.D. (1980). Evidence for multiple intrusion and deformation within the Santa Catalina-Rincon-Tortolita crystalline complex, southeastern Arizona. *Memoir of the Geological Society of America* 153, 217-267.

Kempton, P.D., Fitton, J.G., Hawkesworth, C.J. & Ormerod, D.S. (1991). Isotopic and trace element constraints on the composition and evolution of the lithosphere beneath the southwestern United States. *Journal of Geophysical Research: Solid Earth* 96, 13713-13735.

Kerrich, R. & Rehrig, W. (1987). Fluid motion associated with Tertiary mylonitization and detachment faulting: $^{18}O/^{16}O$ evidence from the Picacho metamorphic core complex, Arizona. *Geology* 15, 58-62.

Lang, J.R. & Titley, S.R. (1998). Isotopic and geochemical characteristics of Laramide magmatic systems in Arizona and implications for the genesis of porphyry copper deposits. *Economic Geology* 93, 138-170.

Lee, S.Y., Barnes, C.G., Snoke, A.W., Howard, K.A. & Frost, C.D. (2003). Petrogenesis of Mesozoic, peraluminous granites in the Lamoille Canyon area, Ruby Mountains, Nevada, USA. *Journal of Petrology* 44, 713-732.

Long, K.B., Gehrels, G.E. & Baldwin, S.L. (1995). Tectonothermal evolution of the Pinaleno-Jackson Mountain core complex, southeast Arizona. *Geological Society of America Bulletin* 107, 1231-1240.

Loucks, R.R., Fiorentini, M.L. & Henríquez, G.J. (2020). New magmatic oxybarometer using trace elements in zircon. *Journal of Petrology* 61.

McGrew, A.J., Peters, M.T. & Wright, J.E. (2000). Thermobarometric constraints on the tectonothermal evolution of the East Humboldt Range metamorphic core complex, Nevada. *Geological Society of America Bulletin* 112, 45-60.

Meijer, A. (2014). The Pinal Schist of southern Arizona: A Paleoproterozoic forearc complex with evidence of spreading ridge–trench interaction at ca. 1.65 Ga and a Proterozoic arc obduction event. *Bulletin* 126, 1145-1163.

Miller, C.F. & Bradfish, L.J. (1980). An inner Cordilleran belt of muscovite-bearing plutons. *Geology* 8, 412-416.

Miller, C.F. & Barton, M.D. (1990). Phanerozoic plutonism in the Cordilleran interior, USA. *Plutonism from Antarctica to Alaska: Geological Society of America Special Paper* 241, 213-231.

Miller, C.F., McDowell, S.M. & Mapes, R.W. (2003). Hot and cold granites? Implications of zircon saturation temperatures and preservation of inheritance. *Geology* 31, 529-532.

Naruk, S.J. (1987). Displacement calculations across a metamorphic core complex mylonite zone: Pinaleno Mountains, southeastern Arizona. *Geology* 15, 656-660.

Otamendi, J.E., Ducea, M.N., Tibaldi, A.M., Bergantz, G.W., de la Rosa, J.D. & Vujovich, G.I. (2009). Generation of tonalitic and dioritic magmas by coupled partial melting of gabbroic and metasedimentary rocks within the deep crust of the Famatinian magmatic arc, Argentina. *Journal of Petrology* 50, 841-873.

Patchett, P.J., White, W.M., Feldmann, H., Kielinczuk, S. & Hofmann, A.W. (1984). Hafnium/rare earth element fractionation in the sedimentary system and crustal recycling into the Earth's mantle. *Earth and Planetary Science Letters* 69, 365-378.

Patiño Douce, A.E., Johnston, A.D. & Humphreys, E.D. (1990). Closed system anatexis in the cordilleran interior: The importance of initial litholoic structure. *EOSTr* 71, 298-298.

Patiño Douce, A.E. & Harris, N. (1998). Experimental constraints on Himalayan anatexis. *Journal of Petrology* 39, 689-710.

Runyon, S.E., Seedorff, E., Barton, M.D., Steele-MacInnis, M., Lecumberri-Sanchez, P. & Mazdab, F.K. (2019). Coarse muscovite veins and alteration in porphyry systems. *Ore Geology Reviews*, 113.

Salas, R.D.R., Ochoa-Landin, L., Ruiz, J., Eastoe, C., Meza-Figueroa, D., Zuñiga-Hernández, H., Mendívil-Quijada, H. & Quintanar-Ruiz, F. (2013). Geology, stable isotope, and U–Pb geochronology of the Mariquita porphyry copper and Lucy Cu–Mo deposits, Cananea District, Mexico: a contribution to regional exploration. *Journal of Geochemical Exploration* 124, 140-154.

Scherer, E.E., Cameron, K.L. & Blichert-Toft, J. (2000). Lu–Hf garnet geochronology: closure temperature relative to the Sm–Nd system and the effects of trace mineral inclusions. *Geochimica et Cosmochimica Acta* 64, 3413-3432.

Schiller, D. & Finger, F. (2019). Application of Ti-in-zircon thermometry to granite studies: problems and possible solutions. *Contributions to Mineralogy and Petrology* 174.

Schmitz, M.D., Vervoort, J.D., Bowring, S.A. & Patchett, P.J. (2004). Decoupling of the Lu-Hf and Sm-Nd isotope systems during the evolution of granulitic lower crust beneath southern Africa. *Geology* 32, 405-408.

Scoggin, S.H., Reiners, P.W., Shuster, D.L., Davis, G.H., Ward, L.A., Worthington, J.R., Nickerson, P.A. & Evenson, N.S. (2021). (U-Th)/He and $^{4}He/^{3}He$ thermochronology of secondary oxides in faults and fractures: A regional perspective from southeastern Arizona. *Geochemistry, Geophysics, Geosystems*.

Seedorff, E., Barton, M.D., Gehrels, G.E., Valencia, V.A., Johnson, D.A., Maher, D.J., Stavast, W.J. & Marsh, T.M. (2019). Temporal evolution of the Laramide arc: U-Pb geochronology of plutons associated with porphyry copper mineralization in east-central Arizona. *Geologic excursions in southwestern North America: Geological Society of America Field Guide* 55, 369-400.

Sharp, Z.D. (1990). A laser-based microanalytical method for the in situ determination of oxygen isotope ratios of silicates and oxides. *Geochimica et cosmochimica acta* 54, 1353-1357.

Shride, A.F. (1967). Younger Precambrian geology in southern Arizona. U.S. Geological Survey Professional Paper 566, 80-89.

Siegel, C., Bryan, S.E., Allen, C.M. & Gust, D.A. (2018). Use and abuse of zircon-based thermometers: a critical review and a recommended approach to identify antecrystic zircons. *Earth-Science Reviews* 176, 87-116.

Silver, L.T. (1955). *The structure and petrology of the Johnny Lyon Hills area, Cochise County, Arizona* (Doctoral dissertation, California Institute of Technology).

Spencer, J.E., Isachsen, C.E., Ferguson, C.A., Richard, S.M., Skotnicki, S.J., Wooden, J. & Riggs, N.R. (2003). U-Pb isotope geochronologic data from 23 igneous rock units in central and southeastern Arizona.

Spencer, J.E. (1984). Role of tectonic denudation in warping and uplift of low-angle normal faults. *Geology* 12, 95-98.

Stevens, G. & Clemens, J.D. (1993). Fluid-absent melting and the roles of fluids in the lithosphere: a slanted summary? *Chemical Geology* 108, 1-17.

Sun, S.S. & McDonough, W.F. (1989). Chemical and isotopic systematics of oceanic basalts: implications for mantle composition and processes. *Geological Society, London, Special Publications* 42, 313-345.

Tang, M., Wang, X.L., Shu, X.J., Wang, D., Yang, T. & Gopon, P. (2014). Hafnium isotopic heterogeneity in zircons from granitic rocks: Geochemical evaluation and modeling of "zircon effect" in crustal anatexis. *Earth and Planetary Science Letters* 389, 188-199.

Terrien, J. (2012). The role of magmatism in the Catalina metamorphic core complex, Arizona: insights from integrated thermochronology, gravity and aeromagnetic data. *Tucson, University of Arizona* (Ph.D. Dissertation).

Teyssier, C. & Whitney, D.L. (2002). Gneiss domes and orogeny. *Geology* 30, 1139-1142.

Thorman, C.H. (1981). Geology of the Pinaleño Mountains, Arizona: a preliminary report. *Arizona Geological Society Digest* 13, 5-12.

Thorman, C.H. & Naruk, S.J. (1987). *Generalized bedrock geologic map and distribution of mylonitic rocks in the eastern Pinaleño Mountains, Graham County, Arizona* (No. 87-614).

Turi, B. & Taylor, H.P. (1971). O^{18}/O^{16} ratios of the Johnny Lyon granodiorite and Texas Canyon quartz monzonite plutons, Arizona, and their contact aureoles. *Contributions to Mineralogy and Petrology* 32, 138-146.

Valley, J.W., Kitchen, N., Kohn, M.J., Niendorf, C.R. & Spicuzza, M.J. (1995). UWG-2, a garnet standard for oxygen isotope ratios: strategies for high precision and accuracy with laser heating. *Geochimica et Cosmochimica Acta* 59, 5223-5231.

Vanderhaeghe, O., Teyssier, C. & Wysoczanski, R. (1999). Structural and geochronological constraints on the role of partial melting during the formation of the Shuswap metamorphic core complex at the latitude of the Thor-Odin dome, British Columbia. *Canadian Journal of Earth Sciences* 36, 917-943.

Vanderhaeghe, O., Teyssier, C., McDougall, I. & Dunlap, W.J. (2003). Cooling and exhumation of the Shuswap Metamorphic Core Complex constrained by $^{40}Ar/^{39}Ar$ thermochronology. *Geological Society of America Bulletin* 115, 200-216.

Vermeesch, P. (2012). On the visualisation of detrital age distributions. *Chemical Geology* 312, 190-194.

Vervoort, J.D., Patchett, P.J., Blichert-Toft, J. & Albarède, F. (1999). Relationships between Lu–Hf and Sm–Nd isotopic systems in the global sedimentary system. *Earth and Planetary Science Letters* 168, 79-99.

Vervoort, J.D., Patchett, P.J., Albarède, F., Blichert-Toft, J., Rudnick, R. & Downes, H. (2000). Hf–Nd isotopic evolution of the lower crust. *Earth and Planetary Science Letters* 181, 115-129.

Vielzeuf, D. & Montel, J.M. (1994). Partial melting of metagreywackes. Part I. Fluid-absent experiments and phase relationships. *Contributions to Mineralogy and Petrology* 117, 375-393.

Wang, D., Fisher, C.M., Vervoort, J.D. & Cao, H. (2020). Nd isotope re-equilibration during high temperature metamorphism across an orogenic belt: Evidence from monazite and garnet. *Chemical Geology*, *551*.

Watson, E.B. & Harrison, T.M. (1983). Zircon saturation revisited: temperature and composition effects in a variety of crustal magma types. *Earth and Planetary Science Letters* 64, 295-304.

Weinberg, R.F., 2016. Himalayan leucogranites and migmatites: nature, timing and duration of anatexis. *Journal of Metamorphic Geology* 34, 821-843.

White, R.W., Powell, R., Holland, T.J.B., Johnson, T.E. & Green, E.C.R. (2014). New mineral activity–composition relations for thermodynamic calculations in metapelitic systems. *Journal of Metamorphic Geology* 32, 261-286.

Wright, J.E. & Haxel, G. (1982). A garnet-two-mica granite, Coyote Mountains, southern Arizona: Geologic setting, uranium-lead isotopic systematics of zircon, and nature of the granite source region. *Geological Society of America Bulletin* 93, 1176-1188.

Zhang, C., Liu, D., Zhang, X., Spencer, C., Tang, M., Zeng, J., Jiang, S., Jolivet, M. & Kong, X. (2020). Hafnium isotopic disequilibrium during sediment melting and assimilation. *Geochemical Perspectives Letters* 12, 34.

Table 1. Sample locations, geochronologic and radiogenic isotopic data.

Sample	Latitude °N	Longitude °W	SiO_2 (wt. %)	Age ± 2σ (Ma)	$\varepsilon Hf_{(t)}$ ± 2σ	$^{87}Sr/^{86}Sr_{(0)}$ ± 1 SE (%)	$^{87}Sr/^{86}Sr_{(i)}$	$^{143}Nd/^{144}Nd_{(0)}$ ± 1 SE (%)	$^{143}Nd/^{144}Nd_{(i)}$	$\varepsilon Nd_{(i)}$
ASH-A	32.75883	-109.87695				0.708602 ± 0.0017	0.708421	0.512593 ± 0.0009	0.512535	-3.0
ASH-1A	32.75883	-109.87695	65.6	54.9 ± 1.5	-4.7 ± 2.4	0.706687 ± 0.0008	0.706448	0.512243 ± 0.0008	0.512207	-9.4
ASH-1B	32.75883	-109.87695	73.0	55.3 ± 2.1		0.707618 ± 0.0007	0.707381	0.512119 ± 0.0012	0.512086	-11.8
ASH-1L	32.75883	-109.87695	74.5	54.5 ± 2.2	-5.8 ± 5.0	0.709639 ± 0.0007	0.709352	0.512165 ± 0.0013	0.512121	-11.1
ASH-2	32.76164	-109.87260	75.3	55.4 ± 2.0	-5.8 ± 2.7	0.708828 ± 0.0008	0.708398	0.512124 ± 0.0007	0.512087	-11.8
SS-20-03	32.75828	-109.87708	62.3	1621 ± 5*						
SS-20-04	32.75560	-109.87955	46.4	1116 ± 19*						
SS-20-06	32.75456	-109.87953	72.2	56.1 ± 2.1	-7.9 ± 5.3	0.708249 ± 0.0007	0.708036	0.512123 ± 0.001	0.512084	-11.8
SS-20-08	32.64895	-109.85996		1445 ± 6*						
SS-20-09	32.73287	-109.82641	72.3	1443 ± 4*						
SS-20-10	32.73518	-109.831	72	1456 ±						

		02		6						
SS-20-12	32.76479	-109.99812	74.5	1638 ± 6						
WILD-1	32.39954	-110.68920	70.1							
WILD-2	32.37722	-110.68720	76.9							

U-Pb ages are weighted means of concordant analyses and U-Pb ages with asterisks are discordia ages derived from the upper or lower intercept on a concordia diagram.

Table 2. Whole rock geochemistry data for samples in this study. Oxides are given in wt. % and trace elements in ppm.

	ASH_1A	ASH_1B	ASH_1L	ASH_2	SS_20_03	SS_20_04	SS_20_06	SS_20_09	SS_20_10	SS_20_12	WILD-1	WILD-2
SiO_2	65.6	73	74.5	75.3	62.3	46.4	72.2	72.3	72	74.5	70.1	76.9
Al_2O_3	16.75	15.6	14.9	14.35	16.85	13.95	15.6	15.85	16.6	12.15	15	14.05
Fe_2O_3	3.53	1.08	0.99	0.99	4.7	17.25	1.44	1.49	1.23	2.45	3.74	0.83
CaO	3.88	2	1.62	1.46	4.68	8.61	2.18	2.66	0.74	1.83	0.71	1.1
MgO	1.86	0.25	0.3	0.15	2.27	5.01	0.42	0.25	0.32	0.54	0.54	0.13
Na_2O	4.49	4.6	4.66	4.32	4.56	0.24	4.79	3.41	4.19	2.97	3.32	3.76
K_2O	2.56	3.72	3.56	3.81	0.7	3.94	2.93	1.98	4.17	3.79	4.42	4
TiO_2	0.48	0.13	0.1	0.07	0.61	2.28	0.19	0.1	0.13	0.45	0.28	0.06
MnO	0.08	0.03	0.03	0.03	0.08	0.27	0.03	0.02	0.01	0.05	0.17	0.06
P_2O_5	0.14	0.04	0.01	0.03	0.25	0.58	0.07	0.06	0.03	0.13	0.03	0.02
La	22.7	23.8	9.6	17.1	25.6	28.1	19.2	51.6	4.6	40.4	25.8	14.9
Ce	45.8	46.8	19.6	33	53.3	64.8	37.1	124	7	89.6	49.7	27.8
Pr	5.5	5.47	2.45	3.9	6.78	9.01	4.53	14.5	0.75	10.3	6.04	3.51
Nd	21.9	19.5	9.2	14.5	27.8	39.3	16.3	54.8	2.5	38.5	22.5	13.2
Sm	3.79	3.31	2.23	2.75	6.5	9.47	3.08	12.95	0.58	7.92	4.95	2.85
Eu	0.85	0.67	0.53	0.65	1.06	2.23	0.61	1.57	1.27	1.53	0.39	0.61
Gd	2.53	1.68	1.51	2.01	3.2	9.87	2.14	15.15	0.7	7.11	3.91	2.74
Tb	0.32	0.18	0.24	0.23	0.97	1.44	0.31	2.68	0.09	1.21	0.63	0.49
Dy	2.19	0.76	1.6	1.36	6.44	9.81	1.73	18.3	0.72	7.17	4.27	3.02
Ho	0.4	0.12	0.3	0.28	1.24	1.98	0.3	3.95	0.15	1.55	0.79	0.65
Y	11.8	4.1	9.4	9	33.4	52.8	8.9	116	4	41.4	24	18.3
Er	1.38	0.35	1.08	1.11	3.7	5.88	0.82	12.55	0.37	4.12	2.59	2.06
Tm	0.17	0.06	0.14	0.18	0.44	0.88	0.11	1.91	0.06	0.73	0.4	0.27
Yb	1.27	0.49	1.05	1.39	2.92	5.62	0.85	12.95	0.35	4.39	2.77	2.12
Lu	0.22	0.08	0.17	0.23	0.42	0.8	0.12	2.06	0.05	0.67	0.38	0.31
Rb	80.6	69.4	67.6	81.6	28.7	192.5	63.9	48.4	90.4	124	205	105.5
Sr	646	565	431	363	643	239	594	287	214	153.5	142.5	301
Zr	110	101	67	170	114	193	98	5	26	207	63	55
Nb	6.6	3.7	5.2	5.1	10.3	9.5	7.7	3	2.1	13.7	25	5.9
Ba	921	1255	1150	1060	213	312	982	983	2320	553	713	1670
Hf	3.1	3.1	2.5	6.4	3.1	4.9	2.9	0.2	0.8	5.8	2.2	1.7

Ta	1.5	1.9	2.5	2.6	1.2	1.3	2.7	1.3	1.6	2.5	2.5	2
Th	4.53	3.83	3.54	4.19	4	1.35	3.82	44.9	0.55	12.35	9.95	5.13
U	1.45	0.9	2.44	2.7	1.54	0.77	1.25	5.1	0.35	3.04	1.51	0.54

Table 3. Selected zircon trace element compositions from the Relleno suite given in ppm.

Sample	Age range (Ma)	Ti	Eu	Hf	Ce	Th	U	U/Th	ΔFMQ
ASH-1A	57–62	4.0–8.3	0.2–1.6	10327–12501	9.3–18.2	29–81	48–116	1.0–1.8	1.2–1.9
SS-20-06	53–58	2.1–4.2	0.4–1.8	12122–22706	23–48	70–380	231–2106	1.9–5.5	1.1–2.6
ASH-2	57–62	1.1–7.1	0.4–1.9	10597–14184	4.1–43.1	12.2–286	74–385	1.3–8.6	0.6–2.5
ASH-1L	56–63	0.9–9.6	0.3–1.3	9771–17025	5.3–20.5	33–116	38–332	1.2–3.6	0.2–2.0

Table 4. Oxygen isotope analyses of mineral separates relative to VSMOW (‰).

Sample	Est. $\delta^{18}O$	$\delta^{18}O$ qtz	$\delta^{18}O$ bt	$\delta^{18}O$ fsp	$\delta^{18}O$ mgt	$\delta^{18}O$ zrc
ASH-1A	6.7	7.2 ± 0.1	4.5 ± 0.1	7.6 ± 0.1	0.7 ± 0.1	4.2 ± 0.1
ASH-1B	6.7	7.4 ± 0.1	4.3 ± 0.1			
ASH-1L	6.4	6.8 ± 0.1	1.0 ± 0.1			
ASH-2	6.6	7.3 ± 0.1	3.6 ± 0.1			
SS-20-06	7.1	9.4 ± 0.1	4.6 ± 0.1	7.1 ± 0.1	-0.6 ± 0.1	

Fig. 1. Regional map of southeastern Arizona showing intrusions of the Laramide arc (green polygons) and southern Arizona anatectic suite (magenta polygons). Inset map shows physiographic provinces of Arizona, Colorado Plateau (CP), Transition Zone (TZ), Basin and Range (BR). Reported ages are zircon U-Pb crystallization ages (Keith et al., 1980; Wright & Haxel, 1982; Goodwin & Haxel, 1990; Long et al., 1995; Lang & Titley, 1998; Fornash et al., 2013; Chapman et al., 2018; this study). MCC = metamorphic core complex.

Fig. 2. Geologic map of the Pinaleño Mountains modified after Thorman & Naruk (1987), and Drewes, (1996). Sample locations are shown with yellow circles with zircon U-Pb crystallization ages.

Fig. 3. A) Schematic outcrop sketch diagram of the Relleno suite showing cross-cutting relationships between phases. Representative sampling locations are shown with number in yellow circles (1 = ASH-1A, 2 = ASH-1B, 3 = ASH-2, 4 = SS-20-06, 5 = ASH-1L). Proterozoic igneous rocks are in light grey (Johnny Lyon granodiorite) and dark grey (dolerite). B) Photo of Phase 2 dikes intruded into Phase 1 pluton. C) Photo of Phase 2 dikes intruded into Proterozoic dolerite.

Fig. 4. Geochemical data of the Relleno suite and other igneous rocks in southern Arizona. A) QAP diagram. B) Aluminum saturation index (ASI) vs. SiO_2 diagram. C) Rock/MORB trace element diagram, and D) Rock/CHUR normalized REE diagram. MORB and CHUR normalizations are from Sun & McDonough (1989). Laramide arc rocks are from Lang & Titley (1998) and Farmer & DePaolo (1984), Wilderness suite rocks are from this study and Force (1997).

Fig. 5. Photomicrographs and representative mineralogy of each of the phases from the Relleno suite including Phase 1 (photo a, sample ASH-1A) Phase 2 (b, c, samples SS-20-06 and ASH-2), and Phase 3 (d, sample ASH-1L). Scale bar in each photos is 500 μm. Kf = potassium feldspar, plg = plagioclase, ap = apatite, qtz = quartz, bt = biotite, msc = muscovite, myr = myrmekite.
Fig. 6. Weighted mean plots and Wetherill concordia diagrams for representative samples of the Relleno suite. Age uncertainties are reported at 2σ.

Fig. 7. Wetherill concordia diagrams for Proterozoic rocks in the Pinaleño Mountains. Age uncertainties are reported at 2σ. Upper and lower intercept ages are reported for discordant samples. The upper intercept age is interpreted to be the crystallization age for each sample and MSWD is reported for the upper intercept age in these cases.

Fig. 8. Zircon/CHUR REE spider diagram and inset Ti-in-zircon crystallization temperature, calculated from Watson & Ferry (2007), vs. U/Th from the same analysis. CHUR normalizations are from Sun & McDonough (1989).

Fig. 9. A) Zircon εHf(t) vs. age plot for Relleno suite samples, the Wilderness suite (red blob) (Fornash et al., 2013), the Texas Canyon stock (blue blob) (Chapman et al., 2018), and Laramide arc rocks (green blob) (Fornash et al., 2013). Crustal evolution lines are shown in blue from 1.0–1.8 Ga, calculated with 176Lu/177Hf = 0.015. B) Samples of the Relleno suite, Wilderness suite (red blob) (Fornash et al., 2013), and Laramide arc (green blob) (Fornash et al., 2013) plotted on

a zircon εHf(t) vs. whole rock εNd(i) diagram with the terrestrial array of Vervoort et al. (1999). The Hf-Nd isotopic decoupling observed in the Relleno suite is a common feature of anatectic rocks (e.g., Zhang et al., 2019).

Fig. 10. A) Plot of εNd(55 Ma) vs. 87Sr/86Sr(55 Ma) for samples of the Relleno suite, amphibolite enclave (ASHA), the Laramide Continental arc (Farmer & Depaolo, 1984; Lang & Titley, 1998) and binary mixing lines between continental mantle lithosphere (CML) (Kempton et al., 1991), Johnny Lyon granodiorite (JLg), and dolerite (Yd) (Bright et al., 2014), and evolved Proterozoic crustal rocks. End members include: 1) Johnny Lyon granodiorite (A. Meijer, personal comm.) and 2) avg. Pinal Schist metapelite (Copeland, 1986) 3) average Oracle granite (Barovich, 1991). B) Quartz δ18OVSMOW values vs. whole rock SiO2 for Proterozoic rocks including the Pinal Schist (blue square) and Johnny Lyon granodiorite (orange square) (Turi & Taylor, 1971), and the Oracle Granite (yellow square) (Kerrich & Rehrig, 1987; Anderson et al., 2005), Laramide arc rocks including the Mariquita Porphyry (green square) and the Texas Canyon stock (red square) (Turi & Taylor, 1971; Salas et al., 2013), and MORB compositions.

Fig. 11. A) Plot of thermometry data vs. whole rock SiO2 content. Zircon saturation temperatures (Tzr, red squares) were calculated from Harrison & Watson (1983), titanium-in-zircon temperatures (Ti-in-zrc, purple diamonds) were calculated from Ferry & Watson (2007), and O isotope equilibration temperatures for quartz-biotite (qtz-bt, green circles), quartz magnetite (qtz-mag, yellow triangles), and quartz-zircon (qtzzrc, blue circle) were calculated from Bottinga (1977), and Botting & Javoy, (1975). B), C), D) Modeled melt compositions of Proterozoic country rock using Perple_X (Connolly 1990; 2005; 2009) compared to compositions of the Relleno suite from this study. Melt compositions are displayed for lithologies of the Johnny Lyon granodiorite (samples SS-20-03, SS-20-12), Oracle granite (samples SS-20-08, SS-20-09, and SS-20-10), and dolerite (sample 0PL95 from Bright et al. (2014)) at conditions of 725 °C, 5 kbar and 825 °C, 10 kbar.

Fig. 12. Probability density plots of the Relleno suite (this study) in the Pinaleño-Jackson Mountain core complex and the Wilderness suite (Fornash et al., 2013) in the Catalina-Rincon core complex using density plotter (Vermeesch, 2012).

Fig. 1.

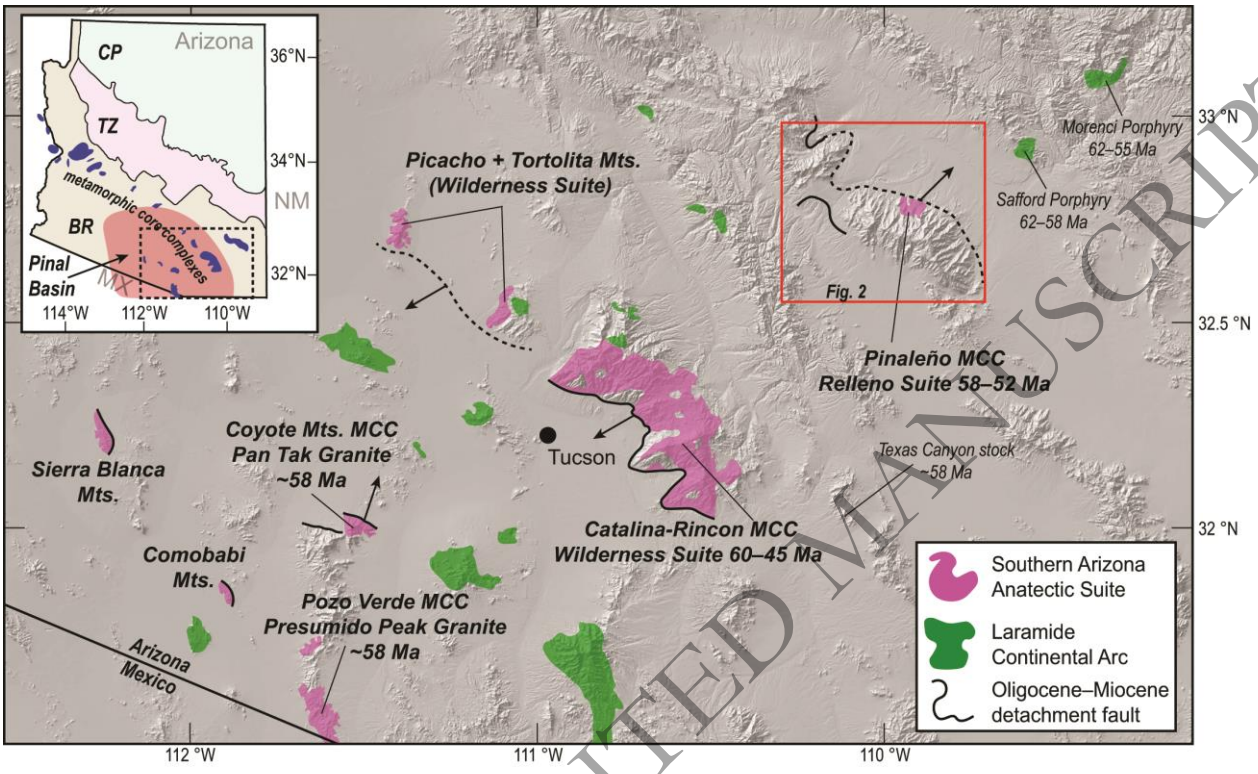

Fig. 2.

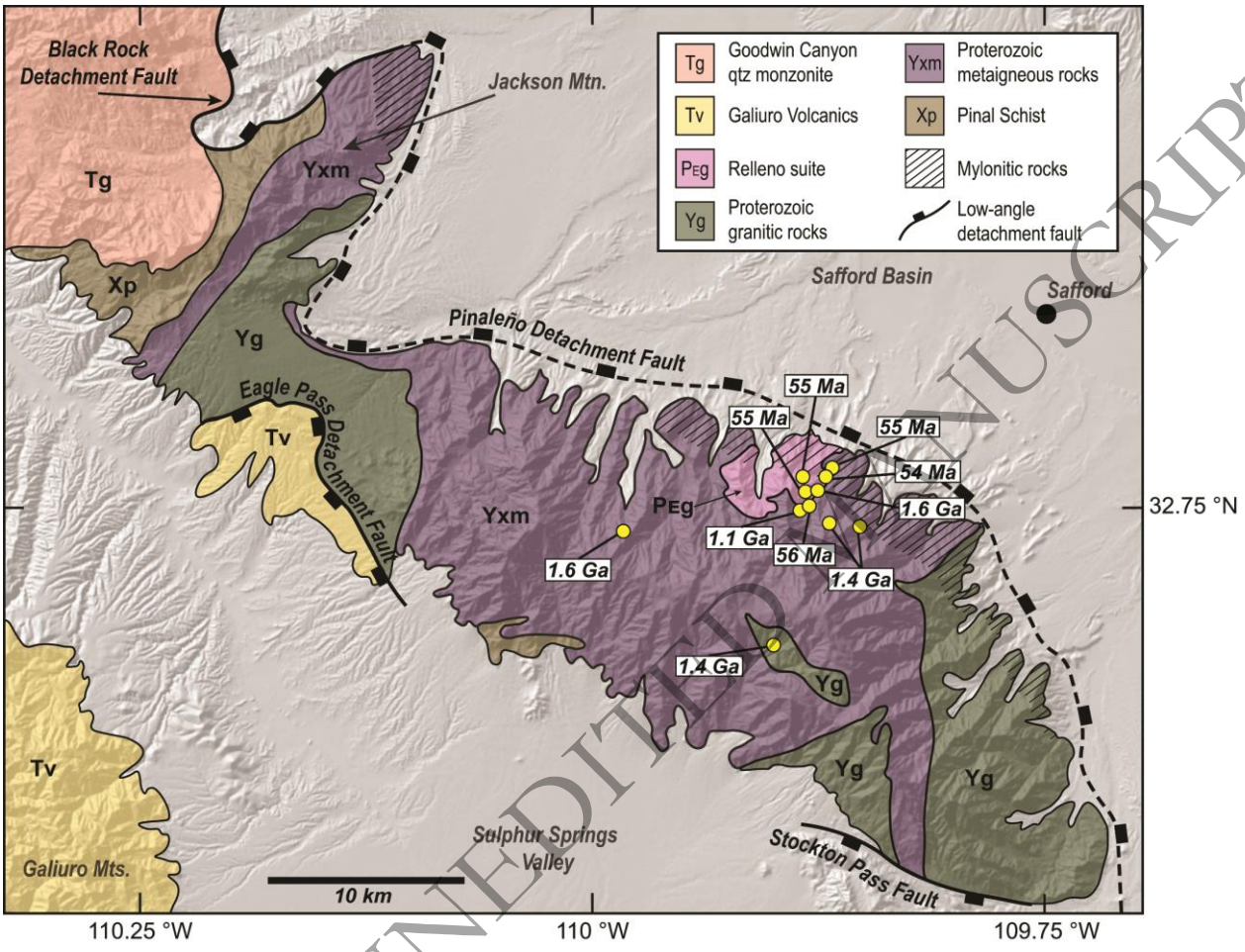

Fig. 3.

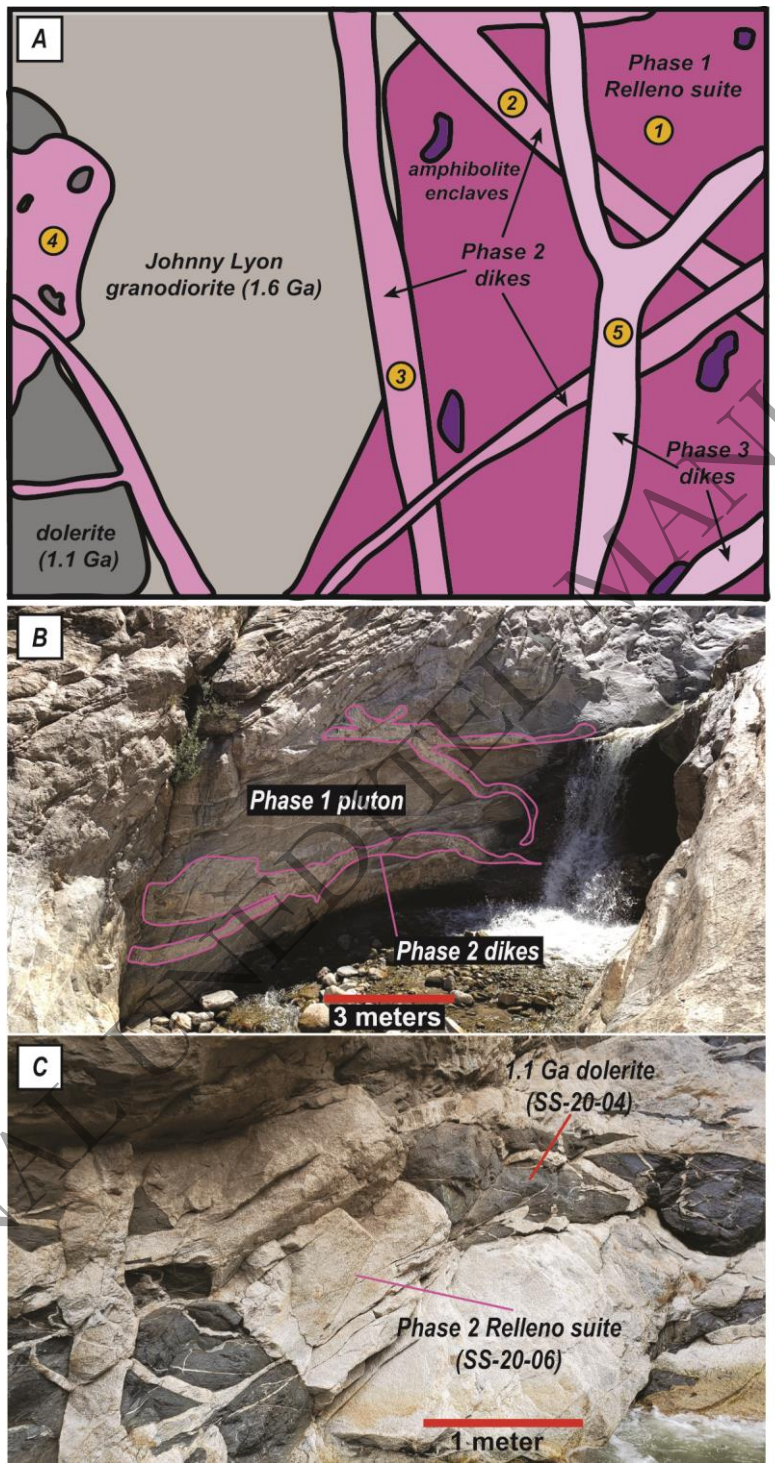

Fig. 4.

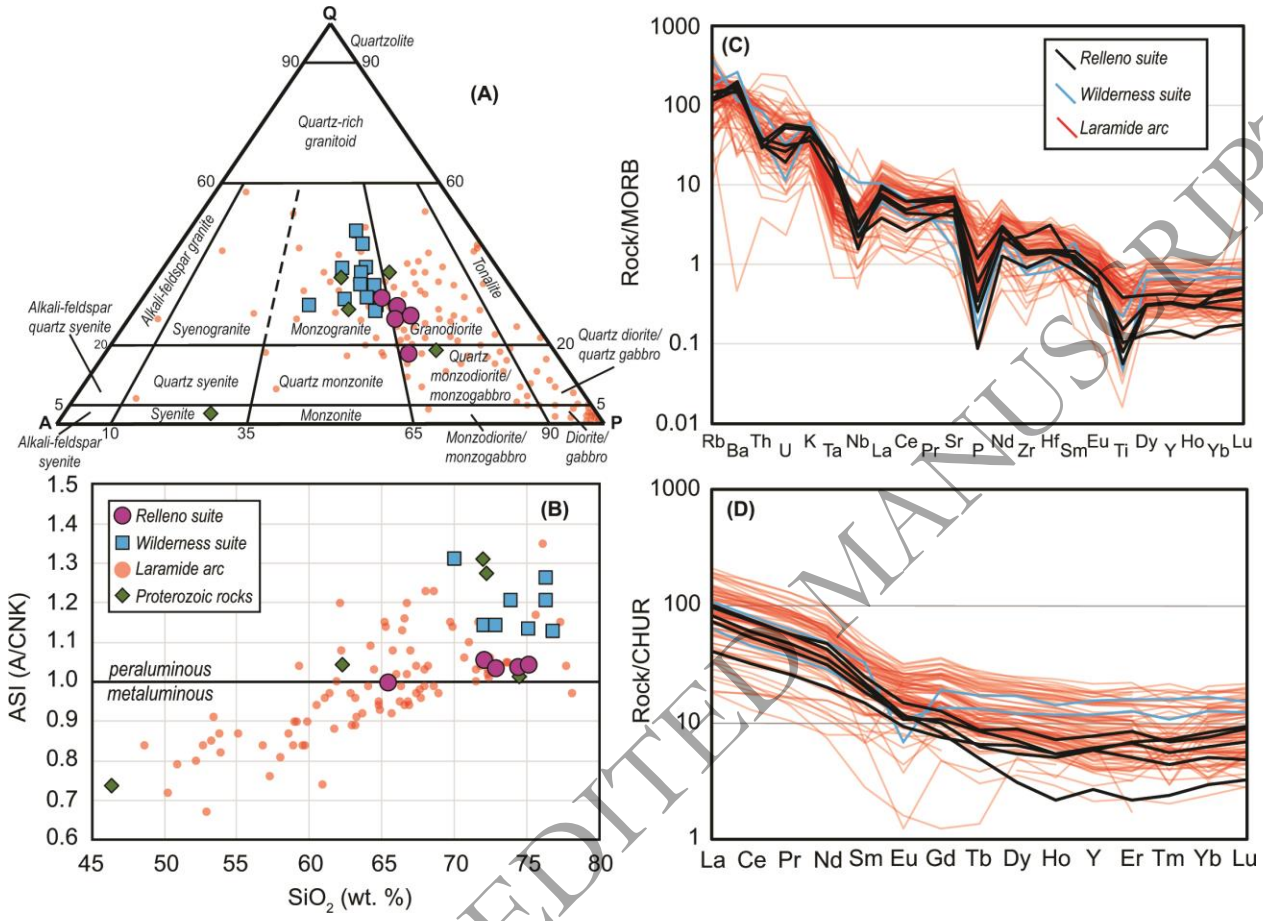

Fig. 5.

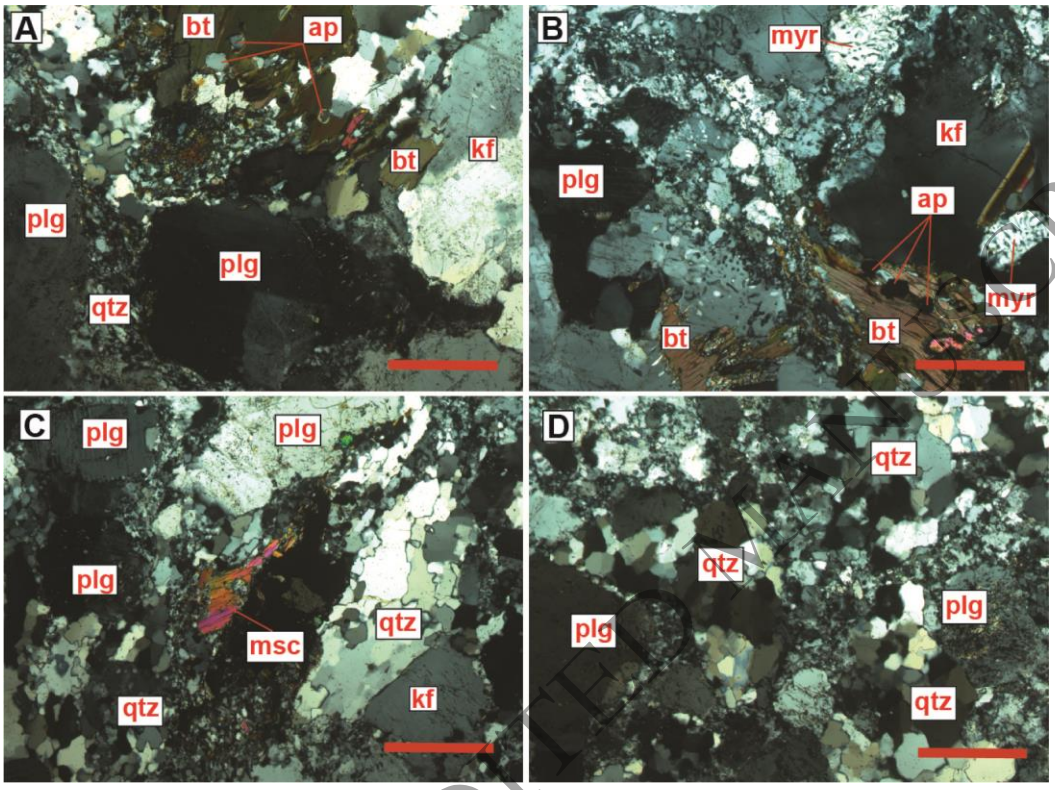

Fig. 6.

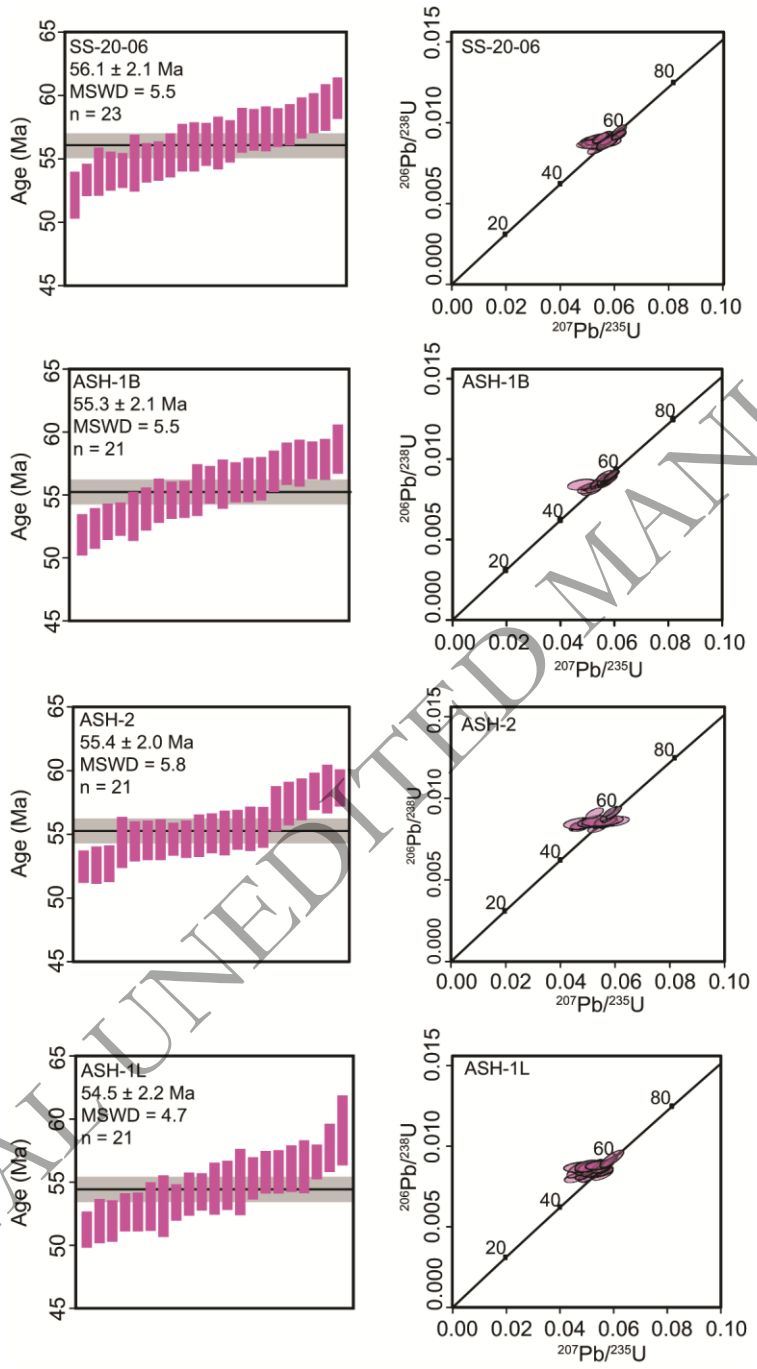

Fig. 7.

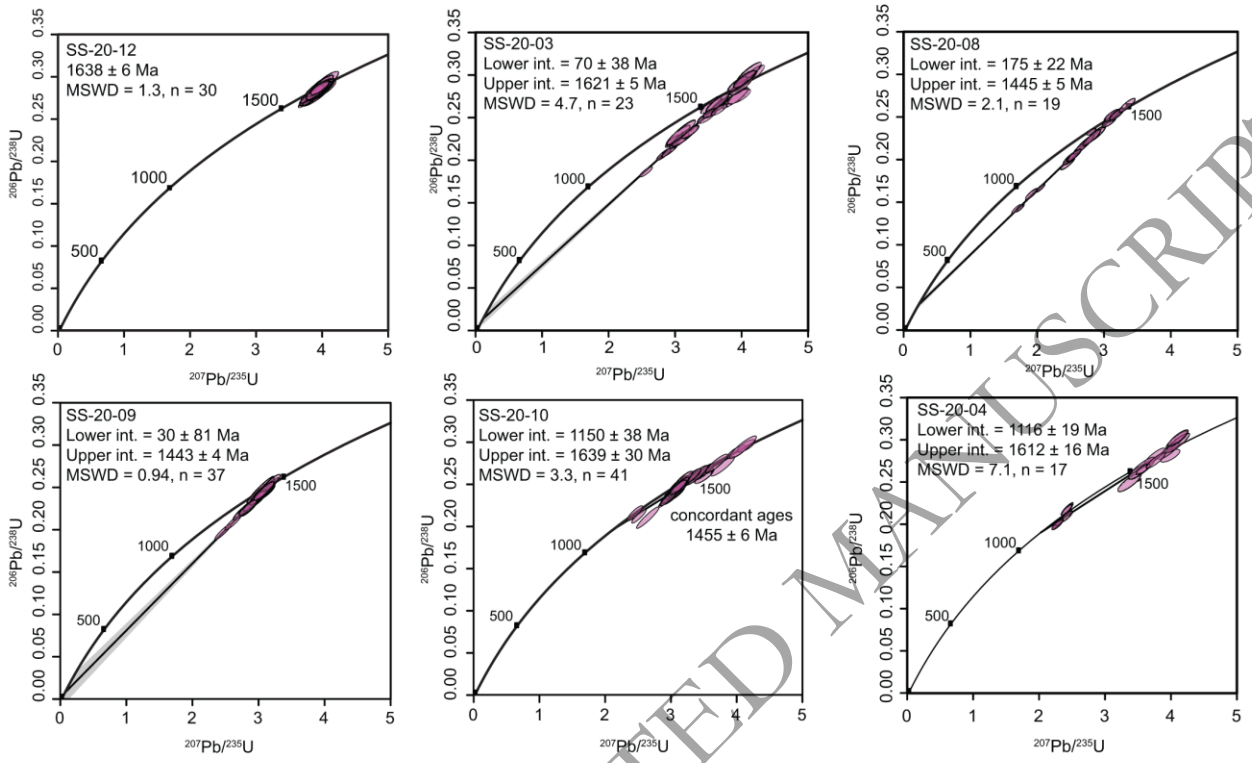

Fig. 8.

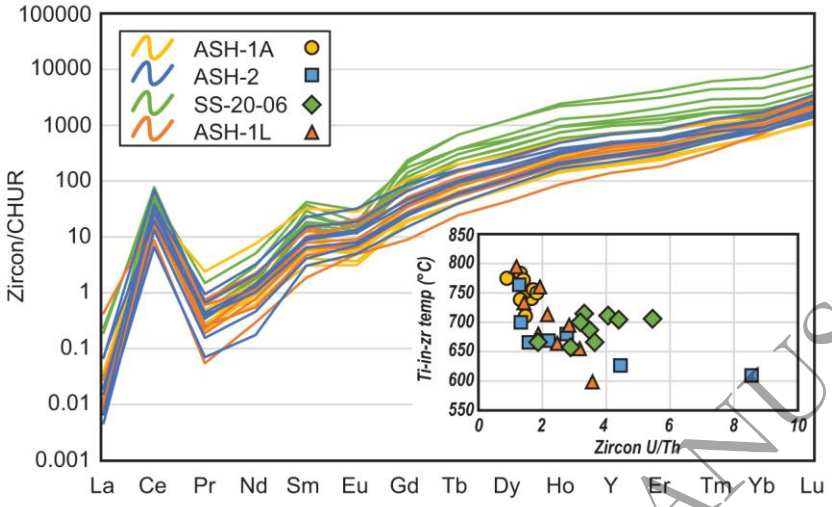

Fig. 9.

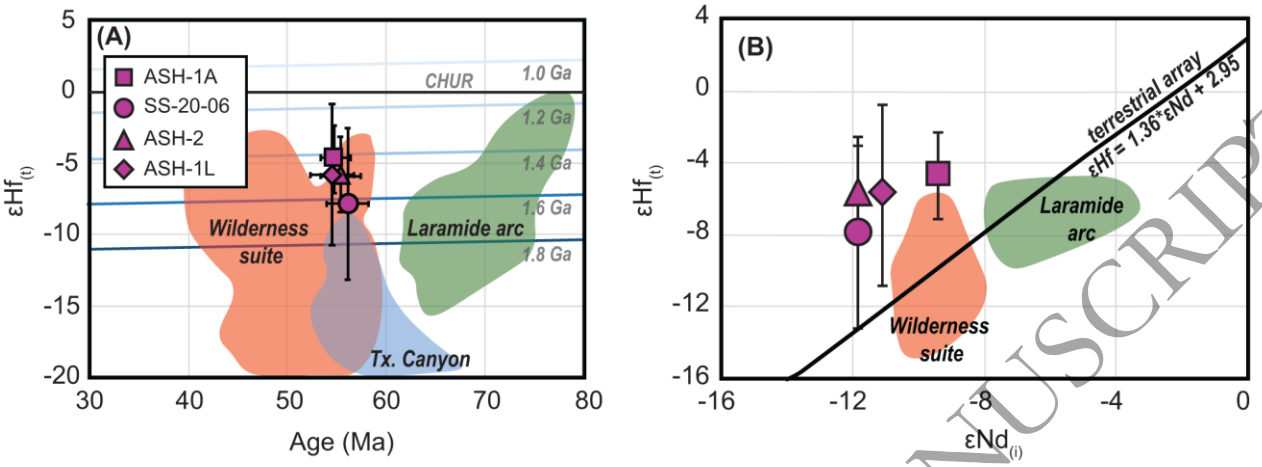

Fig. 10.

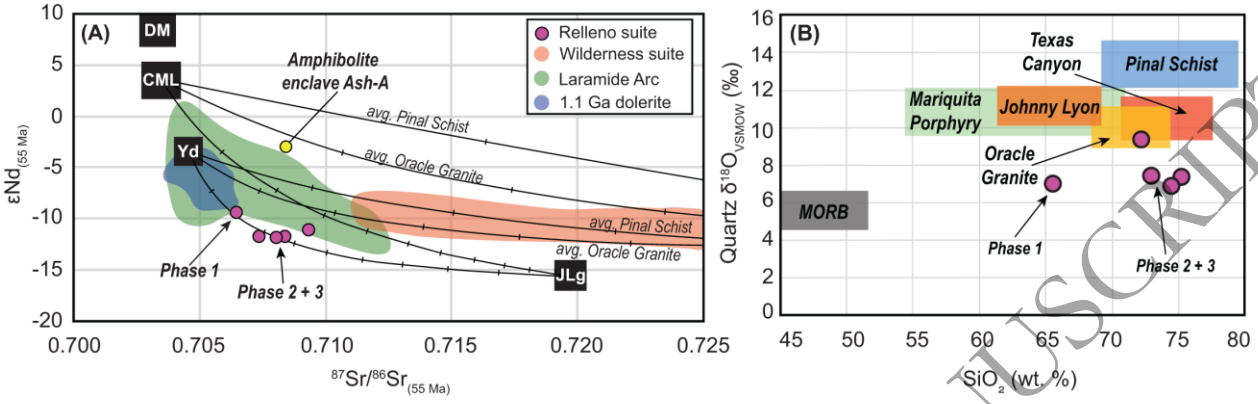

Fig. 11.

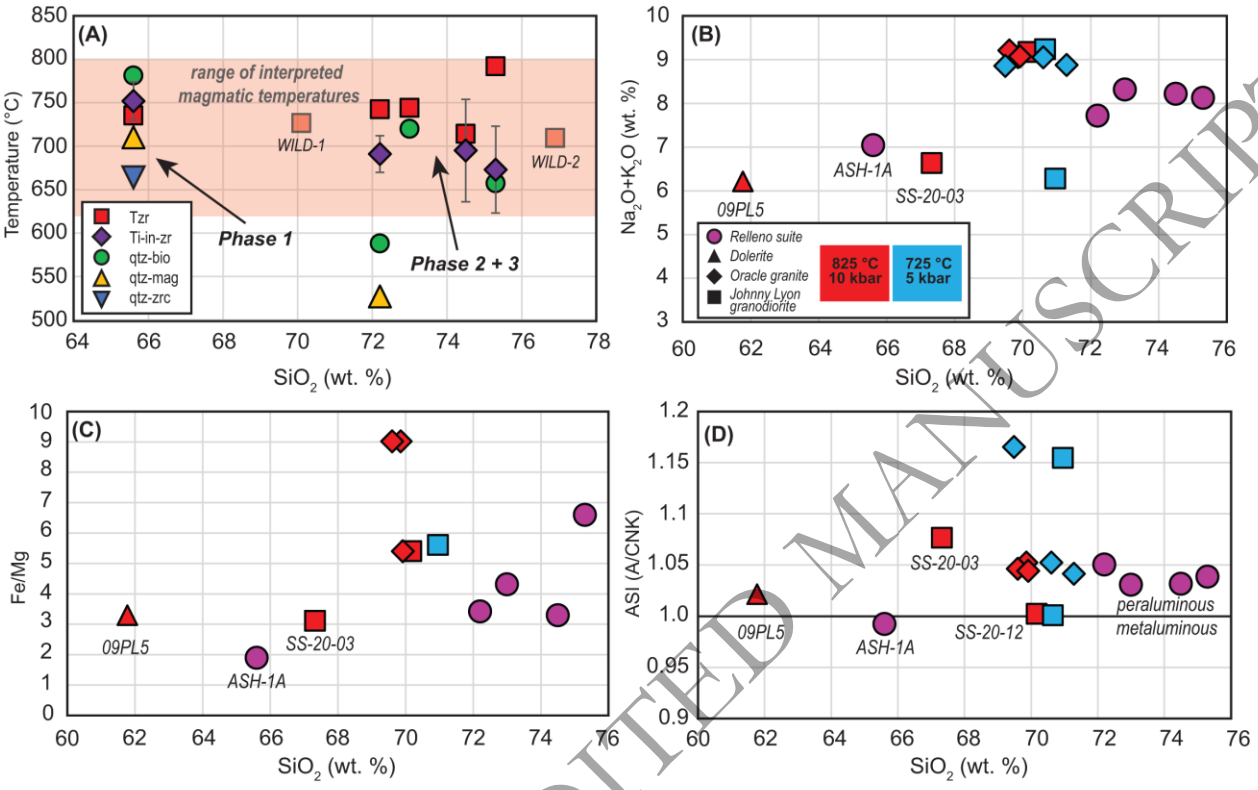

Fig. 12.